FACULDADE DE ENGENHARIA DA UNIVERSIDADE DO PORTO

An Intelligent Retention System for Unmanned Aerial Vehicles on a Dynamic Platform

Lourenço Sousa de Pinho

Mestrado em Engenharia Eletrotécnica e de Computadores

Supervisor: Andry Maykol Gomes Pinto

July 28, 2023

Resumo

Devido aos efeitos cada vez mais negativos dos combustíveis fósseis no meio ambiente, o uso de energias mais limpas é necessário para se atingirem os objetivos de descarbonização acordados na Cimeira sobre as alterações climáticas (COP26). Para atingir este objetivo, existem duas fontes de energia renováveis predominantes, nomeadamente, energia éolica e energia solar. Os parques éolicos são maioritariamente localizados em terra; no entanto, há um número crescente de parques eólicos *offshore*. Estas estruturas apesar de serem cruciais para o desenvolvimento de energia eólica apresentam custos elevados de operação e manutenção, cujo seu valor apresenta 35% do Custo Nivelado de Energia ou *Levelized Cost of Energy* (LCOE). Apesar de serem tecnologicamente avançados, *Unmanned Aerial Vehicles* (UAVs) têm um problema considerável com a sua autonomia energética que só lhes permite voar por curtos períodos de tempo, tendo assim que abortar a missão e aterrar na embarcação sempre que ficar com baixos níveis de autonomia. Esta dissertação visa explorar um novo conceito de inspeção de turbinas *offshore*, com a introdução de plataformas de aterragem capazes de deslocarem-se autonomamente, denominado de NEST (Non-stationary Emersed Structure for Takeoff-landing). O NEST irá ser usado como uma plataforma de aterragem inteligente para que os UAVs possam aterrar após o desenvolvimento da sua tarefa. Adicionalmente, a plataforma deve ser capaz de localizar-se , sendo assim necessários mecanismos de auto-localização. Por fim, devido ao movimento irregular causado pelas ondas e correntes marítima surge a necessidade de a plataforma possuir atuadores, nomeadamente motores ou propulsores, para que esta seja controlada e estabilizada.

Este trabalho explorou o conceito NEST, desenvolvendo toda a eletrónica e o sistema de controlo e navegação que permitem à plataforma desempenhar operações complexas, como mover-se autonomamente até um ponto previamente definido, *station-keeping* e a capacidade de seguir autonomamente outros veículos marítimos.

Abstract

Due to the increasingly negative effects of fossil fuels on the environment, the use of cleaner energies is necessary to achieve the decarbonization targets agreed at the Summit on Climate Change (COP26). To achieve this goal, there are two predominant renewable energy sources, namely, wind energy and solar energy. Wind farms are mostly located on land; however, there is a growing number of offshore wind farms. These structures, despite being crucial for the development of wind energy, have high operation and maintenance costs, costs that represent 35% of the LCOE. Despite being technologically advanced, UAVs have a considerable problem with their energy autonomy only allows them to fly for short periods of time, thus having to abort the mission and land on the vessel whenever they have low levels of autonomy. This dissertation aims to explore a new concept of offshore turbine inspection, with the introduction of landing platforms capable of moving autonomously, called NEST. NEST will be used as an intelligent landing pad for UAVs to land after performing their task. Additionally, the platform must be able to locate itself, thus self-locating mechanisms are necessary. Finally, due to the irregular movement caused by waves and maritime currents, the need arises for the platform to have actuators, namely motors or thrusters so that it can be controlled and stabilized.

This work explored the NEST concept, developing all the electronics and the control and navigation system that allows the platform to perform complex operations, such as moving autonomously to a previously defined point, station-keeping, and the ability to follow autonomously other marine vehicles.

Acknowledgments

I would like to thank my supervisor, Prof. Dr. Andry Maykol Gomes Pinto, for all their support and know-how that was passed on to me, so the objectives of this work could be achieved.

I also thank the Center for Robotics and Autonomous Systems (CRAS) team of the Institute for Systems and Computer Engineering, Technology and Science (INESC TEC), for the patience and knowledge that they made available to me that allowed me to surpass certain obstacles.

To my friends, who were available to answer any questions outside my area of expertise but nonetheless useful to me.

Finally to my family, for all the dedication, support, and patience in this arduous but joyful path that has been my formation.

Lourenço Sousa de Pinho

Official Acknowledgements

This work is partly funded by the European Union's Horizon 2020 research and innovation programme under grant agreement No 871571 (ATLANTIS).

Lourenço Sousa de Pinho

"Perfection is achieved, not when there is nothing more to add,
but when there is nothing left to take away."

Antoine de Saint-Exupery

Contents

List of Figures

List of Tables

Acronyms

ADAS	Advanced Driver Assistance Systems
ArTuga	Augmented Reality Tag for Unmanned vision-Guided Aircraft
ASV	Autonomous Surface Vehicle
AUV	Autonomous Underwater Vehicle
BVLOS	Beyond Visual Line Of Sight
CAD	Computer-Aided Design
CCW	Counter Clockwise
CW	Clockwise
CRAS	Center for Robotics and Autonomous Systems
ESC	Electronic Speed Controller
GPS	Global Positioning System
HLOS	High-Level Operating System
IMU	Inertial Measurement Unit
INESC TEC	Institute for Systems and Computer Engineering, Technology and Science
LiDAR	Light Detection And Ranging
MARES	Modular Autonomous Robot for Environment Sampling
MBES	MultiBeam Echo Sounder
NEST	Non-stationary Emersed Structure for Takeoff-landing
OWF	Offshore Wind Farm
O&M	Operations and maintenance
POM	Polyoxymethylene
RAVEN	Robotic Aerial Vehicle for any-Environment Navigation
ROV	Remotely Operated Vehicle
RTK	Real Time Kinematics
SENSE	autonomouS vEssel for multi-domaiN inSpection and maintEnance
TriOPS	TRIple Offshore Perception System
UAV	Unmanned Aerial Vehicle
USV	Unmanned Surface Vessel
V2V	Vehicle-to-Vehicle
2D	2 Dimensions

Chapter 1

Introduction

1.1 Context

Wind energy is a predominant source of energy becoming more utilized, having an increase of 35,3% of the energy production between the years 2020 and 2021. Additionally, it represents 21,3% of the total energy production worldwide in the year 2020, with a total of 1.588.586 GWh being provided by wind energy producers [1]. The vast majority of these wind farms are located on land, however, there is an increase in the number of Offshore Wind Farms (OWFs), due to the increased output power related to the stronger wind force and faster wind speed in the high seas. By being on high seas, there is no risk of disrupting the environment around these structures, allowing for longer turbines or blades to be used in these structures, and providing a significant improvement in the amount of energy produced.

In the wind power industry, the expression Operations and maintenance (O&M) references a wide range of activities ranging from administrative activities to asset management, however in the context of this scientific work this definition will be narrower, associated with inspection activities that enhance the performance and reliability of the OWFs. O&M ensures smooth energy production and preservation of equipment lifetime, by ensuring asset availability while taking into consideration the safety of the employees involved. In the case of OWFs, these activities are needed to maintain not only the turbine itself but its foundations as such, annual surveys are to be conducted to inspect the condition of these components [2]. Monitoring and repairing the OWFs are harder and more technically challenging because of the cost of human presence at sea to perform the monitoring of these structures, which represent 80% to 90% of the O&M costs.

To perform the maintenance and monitoring of the OWFs, UAVs are often utilized, since they mitigate the technological challenge that is the inspection and maintenance of these structures. UAVs can effectively inspect wind turbine blades for damage and defects, reducing the need for human technicians to climb the turbines and perform these inspections manually. This not only increases safety for the technicians but it also reduces inspection time and costs.

The main benefits of using UAVs on OWFs are the more frequent and spatially larger access to these structures in short amounts of time, the possibility to mount sensors to the UAV to acquire data, and the improvement to safety measures regarding the manned access to these structures [2].

The decision to use UAVs is mainly the data quality these provide and the easy access they have to certain parts of the structures that humans cannot access. The main challenge this maintenance and monitoring methodology faces is the large area needed to cover and the limited battery capacity of the UAVs leading to short flight durations.

1.2 Motivation

Operating drones Beyond Visual Line Of Sight (BVLOS) has many benefits. BVLOS allows a drone to collect more data in fewer deployments and has a lower cost than traditional methods, for example in offshore wind farm inspection, replacing rope-access inspection with drones operating in BVLOS reduces costs by up to 70% and decreases revenue lost due to downtime by up to 90% [3]. The limited endurance of drones poses a significant challenge in achieving medium or long-duration flights, negatively impacting BVLOS operations and leading to stagnation in their deployment. This research work aims to extend the operational capability of UAVs by proposing a marsupial robot configuration, by the name of NEST. A marsupial robotic system consists of a heterogeneous team where a larger vehicle has the ability to carry a smaller one. Both vehicles cooperate and mitigate their individual limitations and enhance their unique strengths, bringing forth a more capable overall system. NEST is an Autonomous Surface Vehicle (ASV) that is able to transport a UAV for offshore wind turbine inspection. ASVs alone have a restricted point of view and limited access to shallow waters. The UAV can provide an aerial view of the surroundings and increase the environment perception range, providing the ASV with a safer path to navigate. However, UAVs have limited battery power leading to reduced flight durations. The endurance of the ASV is more significant since it can be used as the UAV's base station and transport it to different points of interest while recharging or downloading data. This combination of UAV-ASV can execute longer missions and reach difficult and remote locations, being used for O&M operations.

This thesis presents a floating landing pad for the UAV to land and recharge its batteries while in inspection missions, all while being operated BVLOS. To this effect, the landing pad needs positional stabilization to ensure the safety and integrity of both vehicles, hence the vehicles need to communicate with each other at all times. In this thesis, the landing pad must be able to locate where the UAV is and follow its movements to ensure the UAV can land safely, without compromising the integrity of the vehicles.

1.3 Objectives

This scientific work aims to develop a new concept to enable BVLOS operations of a UAV by developing cooperative landing procedures between the UAV and an autonomous moving platform.

This surface vehicle has motor control and is able to locate itself, as well as the aerial vehicle. It ensures that the landing of the UAV can occur safely and precisely. The objectives of this work include:

- **Obj.1:** Development of a NEST concept which is a floating platform capable of autonomously navigating in the sea to provide support to UAVs performing aerial inspections of OW turbines.
- **Obj.2:** Implementation of multiple autonomous functions for NEST in order to enable station-keeping, waypoint navigation, mission planning and vessel following.
- **Obj.3:** Extensive experiments to evaluate the robustness of the hardware developed to NEST as well as the autonomous capabilities. The experiments were conducted in real environments provided by the ATLANTIS Test Centre.
- **Obj.4:** Provide scientific insights for a publication in the field of autonomous robots.

1.4 Document Structure

In addition to this introductory chapter, the document contains four other chapters. Chapter 2 presents some research concerning the state of the art, including some concepts such as UAVs and ASVs. Section 2.2 focuses on the concept of platooning and a specific application that aligns with the theme of this thesis. Section 2.3 describes the technology of cooperative marsupials that is the foundation of this thesis. Chapter 3 describes the hardware that was used and the system integration of all hardware components as well as the algorithm that was developed and some inherent software features that came along with the hardware, followed by some details about each feature. Chapter 4 describes the results obtained for each functionality of the system during simulations and testing. Chapter 5 describes conclusions taken during this scientific work and improvements that should be done in the future.

Chapter 2

State of the Art

This chapter introduces the main topics introduced in this thesis, namely the concept of platooning, cooperative marsupials, ASVs, and UAVs. Section 2.2 describes the concept of platooning and discusses a method developed for platooning marine vessels. Section 2.3 discusses the use of different configurations of cooperative marsupials, some of their general applications, along with some benefits and disadvantages associated with this concept. Section 2.4.1 provides some general applications for ASVs and some developed vessels for more specific applications. Section 2.4.2 describes some general applications of UAVs and examples of already developed UAVs.

2.1 Introduction

The use of ASVs and UAVs in O&M has become increasingly popular due to the numerous advantages they offer. The use of these technologies in O&M allows for more efficient inspections, enhanced safety, reduced costs, reduced environmental impact, better data collection and analysis, and scalability and flexibility. As such, there has been an increase in the integration of both of these technologies in O&M, for example, for the precise landing of UAVs on ASVs. While ASVs and UAVs offer significant benefits, their successful integration into O&M workflows requires careful planning, adherence to regulatory requirements, and consideration of specific operational needs. Due to these factors, there are currently not many options on the market that accomplish the operational and safety requirements for this type of operation.

2.2 Cooperation strategies for multiple vehicles.

A concept in logistics and transportation called platooning describes the tight grouping of vehicles, usually trucks. These vehicles can synchronize their motions and keep a tight distance from one another thanks to sophisticated communication and control systems that link them. Platooning is primarily used to increase productivity, increase safety, and decrease energy or fuel usage.

The lead vehicle in a platoon sets the pace and directs progress, while the trailing vehicles keep a precise distance and speed from the lead vehicle. Radar systems, advanced driver assistance systems (ADAS), and vehicle-to-vehicle (V2V) communication are a few of the technologies used to achieve this cooperation. Platooning is an extremely versatile concept, capable of being applied in many different industries, for example, road vehicles [4, 5], commerce transportation [6], autonomous vehicles, either aerial vehicles [7] or ground vehicles [8, 9], military operations [10] and maritime robotics [11]. The maritime robotics counterpart of platooning will be more deeply weighed upon.

The main benefits of platooning in maritime robotics are:

- **Enhanced Efficiency**: The operational effectiveness of marine robots can be increased by platooning them so they can coordinate their actions and tasks. Together, the robots can split work, communicate knowledge, and plan routes more efficiently, allowing missions to be completed more quickly and effectively.

- **Increased Mission Range and Endurance**: By operating in a coordinated manner through platooning, maritime robots can increase the duration and range of their missions. The robots may cover greater distances or keep a constant presence in one place by taking turns or working in shifts, which enables more thorough data collection or monitoring capabilities.

- **Cooperative Sensing and Information Sharing**: Maritime robots may exchange information and sensor data in a platoon in real-time. Because each robot may contribute its own observations and data, cooperative sensing enables a larger and more thorough awareness of the environment. The robots can jointly produce a more precise and in-depth image of the maritime region by pooling their sensor data.

- **Improved Safety and Redundancy**: Systems for maritime robot platoons can increase redundancy and safety. The robots can operate as backups for one another by staying in tight formation, offering redundancy in the event of faults or failures. The other robots may be able to assume its tasks if one runs into trouble, maintaining mission continuity and lowering the possibility of single-point failures.

- **Resource Optimization**: The pooling of resources among maritime robots is made possible by platooning. For instance, robots in a platoon can share batteries or power supplies to lower the total amount of energy needed. Increased operational efficiency and longer mission durations may result from this resource optimization.

- **Scalability and Flexibility**: Robot systems for the maritime industry can be flexible and scaled thanks to platooning. A platoon's capabilities and operational range can be simply increased by adding more robots. Similarly to this, the platoon can modify its formation or redistribute jobs among the robots if the mission's requirements change.

Figure 2.1: Four truck platooning to reduce fuel consumption

Organizations and researchers can increase operational effectiveness, improve mission capabilities, and make better use of resources by utilizing platooning in maritime robotics. However, while adopting platooning in the maritime realm, it is crucial to take into account aspects like communication reliability, environmental circumstances, and regulatory considerations.

Du et al. [11] propose a High-Level Operating System (HLOS) based method for platooning Autonomous Surface Vessels, where a manned vessel is followed by an unmanned vessel.

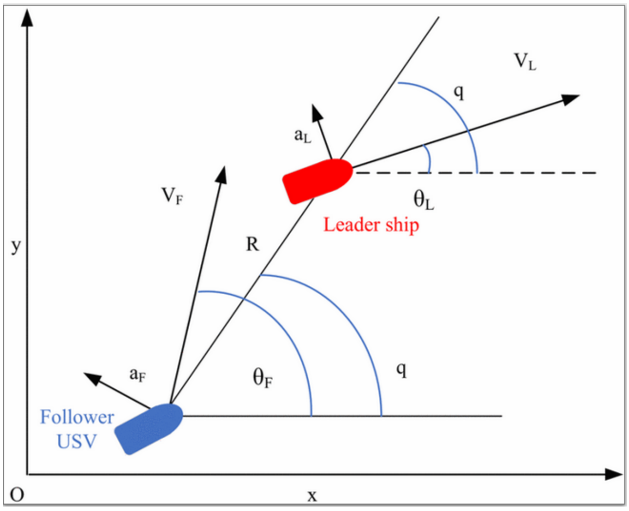

Figure 2.2: The leader vessel and follower Unmanned Surface Vessel (USV)'s positions and velocities diagram [11]

Some of the components required to characterize the interaction between the two vessels are shown in figure 2.2, where q is the angle between the two vessels and R represents the distance between the two. The follower USV and the leader ship's velocities are denoted by V_F and V_L, respectively, while the angles between each vessel's orientation and the x-axis are denoted by θ_F

and θ_L. The accelerations of the leader vessel and follower USV, which are counterclockwise perpendicular to their respective velocities, are a_L and a_F, respectively. $\dot{\theta}_F = a_F V_F^{-1}$ and $\dot{\theta}_L = a_L V_L^{-1}$ are the values obtained. The platooning method's major task is to create a guidance law that gives follower USV reference heading angle θ_F^r , angular velocity $\dot{\theta}_F^r$ and velocity V_F^r.

With these components, the kinematics expression can be expressed, with $\dot{R}$ the approach velocity of one vessel to the other, and $\dot{q}$ being the differential component of the angle between the vessels.

$$\dot{R} = V_L cos(\theta_L - q) - V_F cos(\theta_F - q) \tag{2.1}$$

$$\dot{q} = R^{-1}[V_L.sin(\theta_L - q) - V_F.sin(\theta_F - q)] \tag{2.2}$$

To make the follower USV track the leader vessel in an optimal trajectory, a reference θ_F^r is defined. Afterwards $\dot{\theta}_F^r$ is correlated with the proportional, derivative, and integral terms of $\dot{q}$, as shown in the equation below:

Using $\dot{\theta}_F^r$ as the reference, then the angular velocity that needs to be applied to the follower vessel so that the two vessels are aligned is given by the following equation, possessing the common form of a PID controller, with $k1\dot{q}$ being the proportional component, $k2\ddot{q}$ being the derivative component and $k3\int_{t_0}^{t_{tf}} \dot{q}\,dt$ the integral component.

$$\dot{\theta}_F^r = k1\dot{q} + k2\ddot{q} + k3\int_{t_0}^{t_{tf}} \dot{q}\,dt \tag{2.3}$$

By using all these equations together, the linear and angular velocity of the follower vessel can be acquired and platooning can be achieved. This method will be directly compared to the work developed in this thesis since both tackle the issue in a similar way and serve as a good comparison method for the results.

2.3 Cooperative Marsupials ASV-UAV

A cooperative marsupial robotic system is composed of a larger vehicle and a smaller vehicle, where the larger vehicle can carry the smaller one. By using this approach we can mitigate the constraints of each vehicle and enhance each of the strengths corresponding to each vehicle. These systems are useful for operations in locations that are hard to access, for example, search and rescue missions in catastrophic scenarios, such as the aftermath of Hurricane Wilma [12], urban search and rescue [13] or surveying and inspection of freshwater ecosystems [14].

For maritime robotics, the most common setup for a marsupial robotic system is the combination of an ASV and a Remotely Operated Vehicle (ROV). Another configuration is that of an ASV and a UAV, where the UAV provides an additional viewpoint to the ASV from above, improving the quality of navigation and the ASV provides the UAV with a landing platform from where it can land or takeoff at any time to conserve its battery life, as it can be deployed only when strictly necessary [12]. As such, this setup is capable of executing long and arduous missions efficiently while being capable of reaching remote locations, as well as being used as an inspection or surveying system for analysis or maintenance of structures or search and rescue vessels useful, for example, in natural disasters or accidents in the sea. Figure 2.3 depicts a marsupial UAV-ASV.

Figure 2.3: A marsupial robotic team comprised of a UAV and an ASV [15]

For instance, the ATLANTIS project [16], which is supported by the EU's Horizon 2020 framework, aims to further the development of robotics-based solutions for the inspection and maintenance of offshore wind farms. In particular, marsupial systems are being created in this effort. The marsupial developed for this project is shown in Figure 2.4, which is composed of one ASV constituted by three vehicles, two ASVs, NEST and NAUTILUS, and a UAV, RAVEN (Robotic Aerial Vehicle for any-Environment Navigation), fully developed by CRAS of INESC TEC. The NEST is a passive floating pad, which will be modified in order to enable dynamic navigation, with autonomous navigation capabilities. The NEST is a platform with an omnidirectional thruster configuration, possessing 4 thrusters with a maximum forward thrust of 5.25 kg f and a maximum reverse thrust of 4.1 kg f with a nominal voltage of 16 V. The NEST also has access to a Real Time Kinematics (RTK) Global Position System (GPS) and an Inertial Measurement Unit (IMU), allowing for direction and position acquisition. It is designed to follow vehicles in O&M missions and is capable of performing complex movements and procedures. Additionally, the NEST has in its structure a multimodal artificial marker ArTuga (Augmented Reality Tag for Unmanned Vision-Guided Aircraft)[1], proposed by Claro et al. [17]. The UAV RAVEN is composed of a visual and thermal camera and a 3D LiDAR, this group of sensors comprises the system known as TRIple Offshore Perception System (TriOPS) [17]. With this system, the UAV is able to detect the ArTuga, and consequently, the landing platform, which allowed for the conduction of tests in maritime environments, more specifically in the marine of Viana do Castelo, Portugal.

[1] Patent pending (Portuguese Patent Request (PPP) nr. 118328, and European Patent Request (EP) nr. 22212945.4)

Figure 2.4: Marsupial Robotic team developed by CRAS.
The black vessel is the NAUTILUS, the UAV is the RAVEN and the floating pad is the NEST.

A cooperative perception system acquires information utilizing individual vehicles and shares it with other vehicles, thus extending the range of perception that each vehicle perceives [18]. This principle is useful in a great number of scenarios, the most relevant being obstacle avoidance as this allows the UAV, for example, to identify obstacles that the ASV cannot perceive and share that information, allowing for safer and more efficient navigation. Another advantage of cooperative perception is the reduced cost it provides in comparison to conventional long-range sensors [18]. To achieve cost savings, a strategy involves equipping the UAV with affordable long-range sensors while outfitting the ASV with less expensive short-range sensors. By sharing the information obtained between them, this approach reduces the sensor costs compared to using more advanced and expensive sensors while still achieving comparable results.

Rather than transmitting all the gathered data to a central node for state estimation, an alternative approach involves processing the information at the individual acquisition points and subsequently combining it into the central node for fusion [19]. This method allows for more flexibility, i.e. allows for a high number of nodes without reliability degradation or communication overhead; is more robust to failures and has a reduced communication cost [19]. Figure 2.5 depicts the cooperative perception principle when applied to a UAV and an ASV.

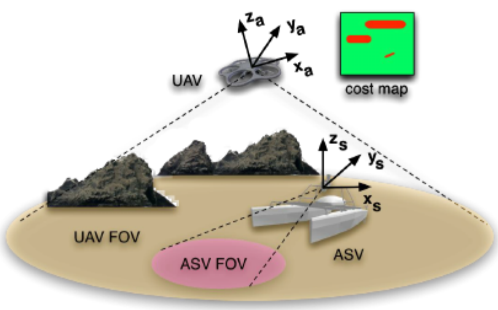

Figure 2.5: Cooperative perception principle [15].

To obtain a precise awareness of the environment, the data that is obtained needs to be correctly fused [19], allowing for an accurate and absolute representation of what is perceived in the surroundings, thus ensuring a safe, efficient, and reliable deployment.

2.4 Robotic platforms towards aerial inspections BVLOS

2.4.1 Autonomous Surface Vehicles

ASVs are an important area of research in the field of maritime robotics, as they have the potential to revolutionize a variety of marine applications with environmental monitoring[20], search and rescue[20, 21], oil spill response[22], structure inspection [23, 24, 25, 26, 27, 28] and vessel detection [29] as some examples. One key area of research on ASVs has been the development of robust and reliable control algorithms for tasks such as obstacle avoidance and path planning. Researchers have explored a variety of approaches to these problems, including the use of sensors such as LiDAR and radar, as well as more complex methods such as artificial neural networks[30] and fuzzy logic[31].

Another important area of research has been the integration of ASVs with other systems, such as UAVs and Autonomous Underwater Vehicles (AUVs) [32, 33], to create hybrid systems with enhanced capabilities. Researchers have focused on developing methods for communication and coordination between the different platforms, as well as on integrating multiple sensors and data sources to enable more complex mission scenarios.

ASVs can map and obtain accurate representations of the terrain above and below sea level. This is done by combining data obtained from underwater sensors, such as sonars or LiDAR systems, with bathymetric data obtained by the ASV and then geo-referencing both data sets [2].

ASVs possess the advantages of agility and rapid response, along with the ability to integrate diverse sensors, allowing for greater control of the vessel and a greater recognition of the environment around them. However, ASVs are subject to specific weather conditions and require certification for joint operations with manned vessels. Coordinated control between ASVs and UAVs becomes necessary for tackling challenging tasks involving real-time navigation and perception [2].

The ROAZ and ROAZ II ASVs, depicted in Figure 2.6, were created as part of a marine robotics project at the Autonomous Systems Laboratory of the Instituto Superior de Engenharia do Porto with the intention of assisting procedures for search and rescue in an aquatic environment as well as for the collection of hydrographic data [34, 35]. To integrate ROAZ II into the most durable version, with dimensions 4.5 m x 2.2 m x 0.5 m intended to operate in the open sea, solutions are tested on ROAZ, which has been designed to function on rivers and estuaries. They both employ a catamaran structure, which ensures good stability and minimal entrainment. An onboard computer on the ROAZ is in charge of mission-related vehicle navigation and control. It has an IMU, GPS, Wi-Fi, a visual camera, and the ability to use several SONAR types. Only a thermal camera has been added to ROAZ II's architectural navigation and perception system. The

ROAZ II was also used to perform cooperative missions with an autonomous underwater vehicle, the MARES (Modular Autonomous Robot for Environment Sampling) [21, 36].

(a) ROAZ ASV

(b) ROAZ II ASV

Figure 2.6: ROAZ and ROAZ II ASV developed by IPP/ISEP [35]

The autonomouS vEssel for multi-domaiN inSpection and maintEnance (SENSE) is a small-sized ASV developed by INESC TEC in Faculdade de Engenharia da Universidade do Porto, being in operation since 2005 [37, 38]. It has a length of 1.5m, a width of 1.1m, and a height of 1.9m, it weighs a total of 50 kg with an available payload of an additional 50 kg. It possesses two trolling motors in a differential drive configuration, has an operation time of approximately 2 hours, being supplied with 3S LiPo batteries. The navigation module, the perception module, and the localization module are the vessel's three available modules. The navigation module is made up of an RTK-GPS, an IMU, and an embedded computer that uses WiFi to connect to the ground station and exchange data with it. Through a PWM motor drive, the inbuilt computer also controls the thrusters. The MultiBeam Echo Sounder (MBES) laser scan, a stereo camera, a 3D LiDAR, and an embedded computer allow the perception data collected to be recorded, and transmitted to the ground station. The localization module offers an additional GPS, IMU, and embedded computer to read the information and determine the vehicle's position. The RTK technology, which may be applied as a localization estimate tool, makes it possible for a more precise localization estimate.

(a) Front View of ASV SENSE [37]

(b) Side view of ASV SENSE[38]

Figure 2.7: INESC TEC's ASV SENSE

Ocean Infinity is looking for low-emission, economically viable marine solutions, and services for a variety of sectors, including offshore energy, logistics, and transportation. It created a fleet of USVs called the Armada, with dimensions 21 m x 36 m x 78 m, depicted in figure 2.8. These vessels can transport a variety of payloads, including AUVs, ROVs, SONAR, and cameras for various mission types, thanks to their monohull configuration. The 78 m series Armada 7801, seen in Figure 2.8, has a 25.928 km/h (7.20 m/s) top speed.

Figure 2.8: Armada 7801 ship

The Blue Essence vessel developed by Fugro and SEA-KIT International is a 12-meter vessel designed for inspecting subsea assets and can be remotely operated from any location in the world. This vessel also incorporates the Blue Volta e-ROV. The vessel's advanced systems are composed of an array of geophysical sensors for subsea inspection asset and site characterization surveys, reducing by 95% the emissions produced when compared to other vessel operations[2].

Figure 2.9: Fugro Blue Essence Vessel

[2] https://www.offshore-energy.biz/fugros-blue-essence-becomes-first-uae-flagged-uncrewed-surfac

2.4.2 Unmanned Aerial Vehicles

UAVs, also known as drones, have gained significant attention in recent years for their potential to revolutionize a variety of applications, including military operations [39], precision agriculture [40], disaster response[41, 42] and wireless networks [43], along with many other applications. Additionally, UAVs have been recently more utilized in the automated inspection of energy assets, such as wind farms or solar farms, because they can sweep large surfaces and areas in a short amount of time. For instance, they are commonly used in large-scale solar farms to monitor the condition of the solar panels and to maintain the best conditions for power generation, since dust can affect the capability to produce energy in a solar farm [2].

Figure 2.10: UAV near Offshore Wind Farm

In the area of inspection and maintenance of wind structures, UAVs are more widely being used, especially in OWFs. These renewable energy facilities are located in harsh and remote environments, making them difficult and costly to access for maintenance and inspection purposes. UAVs offer a cost-effective and safe alternative for performing these tasks, as they can quickly and easily reach areas that are otherwise difficult to access by humans.

While the use of UAVs for offshore wind farm inspections offers many benefits, there are challenges and limitations to consider. One challenge is the limited flight time of most UAVs, which can limit the extent of inspections that can be performed in a single mission. In addition, the reliability and accuracy of UAVs can be impacted by factors such as weather conditions and the condition of the equipment. Finally, there are also regulatory and legal considerations to be taken into account, as the use of UAVs in offshore environments is subject to strict rules and regulations.

The FLYABILITY's Elios 3 is a UAV that is 48 cm wide and 38 cm high, weighing 2.4kg with a maximum payload specifically designed for the inspection of structures. It has a maximum flight time of 12 min without payload and 9 min with payload. It possesses an IMU, a magnetometer, a barometer, LiDAR, 3 computer vision cameras, and a ToF distance sensor. The Elios supports work in dark areas with a dual thermal 4K camera and 16K lumen dust-proof lighting system, allowing it to identify signs of cracking, corrosion, and structural issues[3].

Figure 2.11: FLYABILITY Elios3 UAV

DJI's Matrice 300 RTK is a rugged wind turbine inspection drone built to handle extreme weather conditions. It has dimensions of 810 x 670 x 430 mm weighing approx. 6.3 kg with a maximum takeoff weight of 9 kg. It is capable of integrating various sensors, including visual and thermal cameras. It has a 15 km Max transmission range, with a 55-min max flight time, capable of operating in temperatures between -20ºC and 50ºC, and an IP45 rating.

Figure 2.12: DJI Matrice 300 RTK UAV

[3] https://www.flyability.com/elios-3

The RAVEN[17] is a VTOL UAV based on a hexacopter frame, with a wingspan of 1.6 meters and a maximum payload of 10 Kg, equipped with a PixHawk controller running the ArduPilot software. The GNSS/RTK sensor that makes up its navigation system has a positioning accuracy of 2.5 m and 0.01 m when connected to a base station. It is equipped with an inbuilt processor that is an Aetina AN110-XNX with an NVIDIA Jetson Xavier NX Module. Four 6 S 30,000 mAh semi-solid Li-Ion batteries power RAVEN, giving it a minimum flight time of 50 minutes (depending on the payload). It is equipped to perform various O&M functions, allowing for the close-range inspection of wind turbines and structural inspection and assessment of the wind turbine's structure, for example, thermographic inspection and biofouling.

Figure 2.13: UAV RAVEN[17] developed by CRAS of INESC TEC

2.5 Critical Review

The NEST concept aims to solve the problem of the autonomy of UAVs, allowing them to land on a dynamic platform after the completion of their operations. This approach makes it possible to carry out longer missions and increases the efficiency of the operation. Upon reviewing the current state of the art, it becomes apparent that UAV technology possesses certain limitations that warrant further exploration and the development of effective countermeasures to these limitations. Moreover, various existing technologies have emerged to address these limitations, presenting a diverse range of potential solutions. By leveraging these solutions, the process of solution development is streamlined, enabling more efficient and seamless progress in addressing the challenges at hand.

Chapter 3

The NEST concept for enabling UAV-ASV interactions

The NEST concept comprises autonomous platforms designed to offer logistical support to UAVs, addressing their limited battery capacity. These platforms serve as landing pads for the UAVs, facilitating battery charging and data transfer between the two vehicles. This thesis primarily emphasizes the development of the NEST, encompassing aspects such as its kinematics, localization, and autonomous functionalities like station-keeping and waypoint navigation. Additionally, it explores the establishment of a cooperative framework between the UAV and NEST for enhanced performance.

Figure 3.1: NEST Floating pad

Figure 3.2 illustrates the fundamental concept of NEST along with an illustrative depiction of the potential operational scenario that prompted its inception.

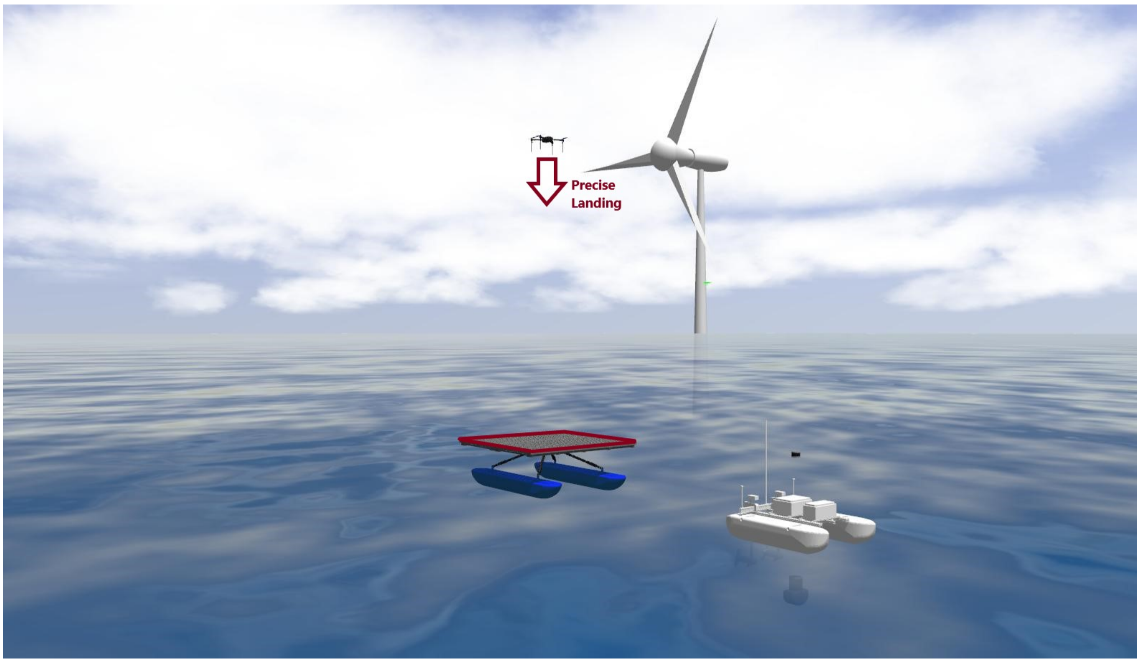

Figure 3.2: NEST application scenario

3.1 Hardware Architecture

This section covers every aspect of the hardware used in the system, including the preparation required for its construction. The energy module and the control module are the two most important components in the hardware configuration. The power elements required to sustain the entire system are stored in the energy module. Batteries, which supply the required electrical energy, and connectors, which establish smooth communication between the two modules, are included in this. The technology ensures a consolidated and effective approach to power management by housing these power elements within the energy module. The control module, on the other hand, is in charge of enabling autonomous operation. It includes a variety of essential components, such as microcontrollers, sensors, and actuators like thrusters, which lets the system react to its surroundings and carry out activities on its own. The system creates a compact and coherent structure that allows effective and efficient autonomous functionality by combining these parts into the control module. Figure 3.3, which shows how the various components are separated and connected, has been provided to give a visual depiction of the system architecture.

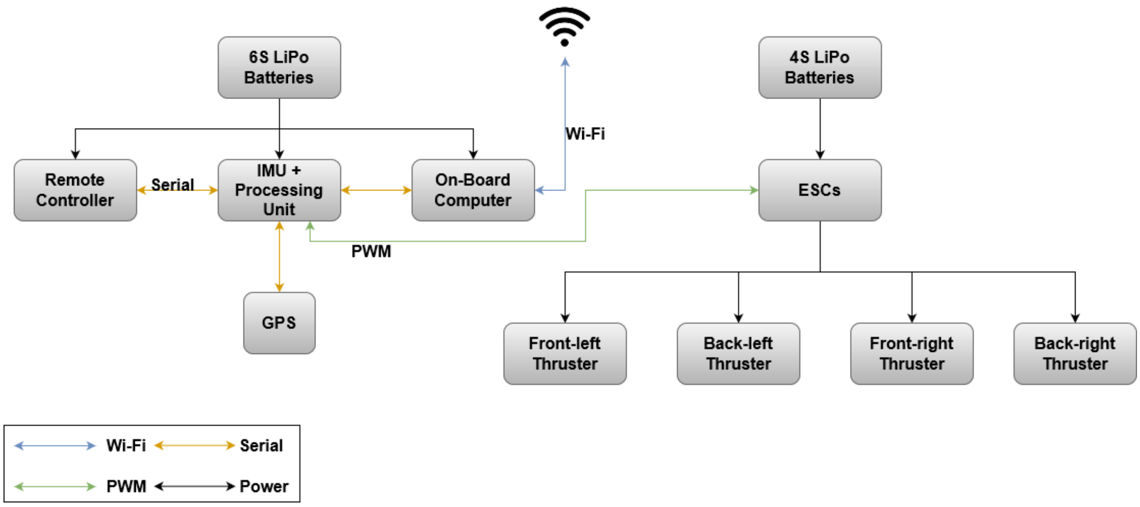

Figure 3.3: Hardware Architecture

3.1.1 Energy Module

Given the substantial energy demands of the entire system, ensuring the appropriate design of the energy module is crucial for its optimal functioning. Therefore, careful consideration must be given to the selection of batteries, their capacity, and the storage method. Prior to enabling the system to operate, it was imperative to provide it with the requisite voltage and current. In this scenario, an energy module was developed with a maximum power usage of 600 Wh, which was divided into two levels: 14.8 V for thruster operation and 22.2 V for the control module. The thrusters have an ideal working nominal voltage range of 12-16 Volts, while the maximum drawn current is 24 Amps. To fulfill these requirements, four 4S LiPo batteries were utilized, each with a nominal voltage of 14.8 Volts and a maximum capacity of 16,000 mAh. As for the control module, three 6S LiPo batteries were selected, each with a nominal voltage of 22.2 Volts and a maximum capacity of 16,000 mAh.

To power the Processing Unit, we connect a step-down converter with a maximum voltage rating of 8S to the 6S batteries. This converter ensures compatibility between the batteries and the Processing Unit. To supply the Remote Controller and On-board Computer, which require a 12 Volt input, we employ a step-down converter capable of converting 15-40 volts to 12 Volts/5 Amps. As the optimal operational voltage for the thrusters is 16 Volts, the 4S LiPo batteries are utilized to power the Electronic Speed Controllers (ESCs). These batteries provide the necessary power for the thrusters and provide an interface with the Processing Unit.

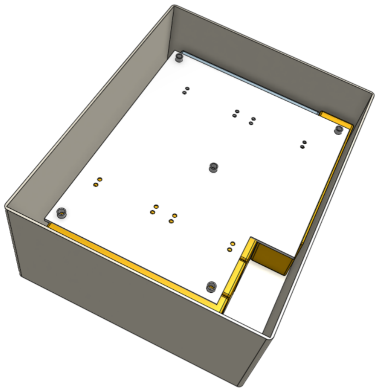

(a) Battery Box with battery cover

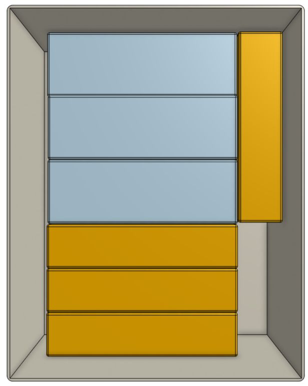

(b) Battery Box without battery cover

Figure 3.4: Battery Box (Blue batteries are 6S and yellow batteries are 4S)

Figure 3.4 shows an approximation of the box in which the batteries are stored, with dimensions of 325x254x130 mm to carry the 217x120x65 mm 6S batteries and 192x75x65 mm 4S batteries. The holding pad, shown in white in figure 3.4a, was created using 3D printing technology. This holding pad is then placed on top of the batteries to keep them from moving around inside the box thus preventing accidents or damage to the batteries. There are two terminals on the holding pad that serve as the connectors' interface. Each one had a certain type of battery allocated to it, and that type's batteries were connected in parallel to provide an output with the same voltage as the battery type but a higher output current that could be used how the system saw fit. Figure 3.5 depicts the battery box after it has been fully developed. Figure 3.6a shows the positive and negative terminals of each battery type and figure 3.6b shows the connectors used to connect the two modules. Since the system that will be in contact with water at all times, there is a need to safeguard the equipment against it, maintaining the integrity of the vehicle. The requirements for the connectors and box are shown in Table 3.1 to ensure that there is no water leakage, preventing water damage and averting accidents.

Component	**Requisites**
Box	IP Classification: IP68
Connectors	IP Classification: IP68 Voltage: 24V Current: 25A per pin

Table 3.1: Requisites for the box and connectors of the energy module

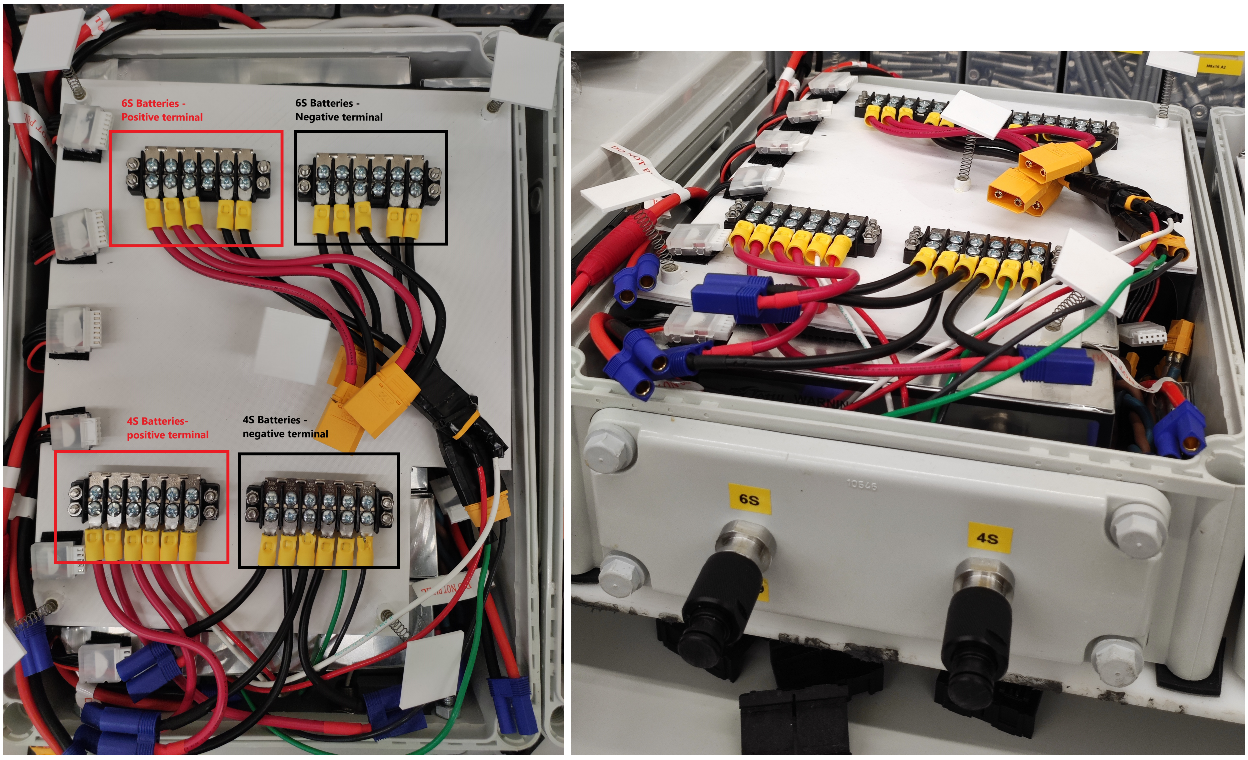

(a) Battery box with terminals specified

(b) Battery Box with connectors

Figure 3.5: Final product of Battery Box

3.1.2 Control Module

For the system to properly function autonomously, sensors and actuators were used as well as processing power capable of handling all data obtained by the sensors and needed by the actuators. For this effect, the Control module was developed, being initially composed of an embedded computer, namely the ODROID N2+, an RTK-GPS, an RC Controller, and an autopilot with an inbuilt IMU, namely the PixHawk CubeOrange+. A 380 x 190 x 130mm box with an IP68 rating was chosen as the holder for the components of the Control Module in order to prevent water damage and electrical mishaps.

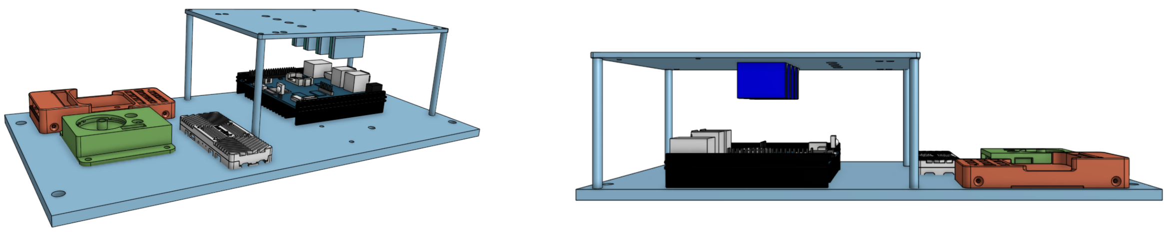

(a) Control box top view

(b) Control Box side view

Figure 3.6: Designed Control Box

Figure 3.6 shows the design of the control module's components and some designed pieces that were added to the box, with the use of Computer-Aided Design (CAD). In light blue we have the designed pieces, the bottom one was later made out of a piece of POM (Polyoxymethylene) plastic, often known as acetal plastic, which has dimensions of 325 x 164 x 6mm. The top piece was later 3D printed with dimensions of 185 x 120 x 3mm, with 4 30 x 25 x 3mm edges to hold the ESCs, as shown in figure 3.7. The elements that were utilized are depicted in color. The autopilot, a PixHawk CubeOrange+, is orange, the RTK-GPS is green, the RC controller is white, the ESCs are dark blue, and the ODROID N2+ is black, blue, and white, while the CAD-designed pieces are depicted in light blue.

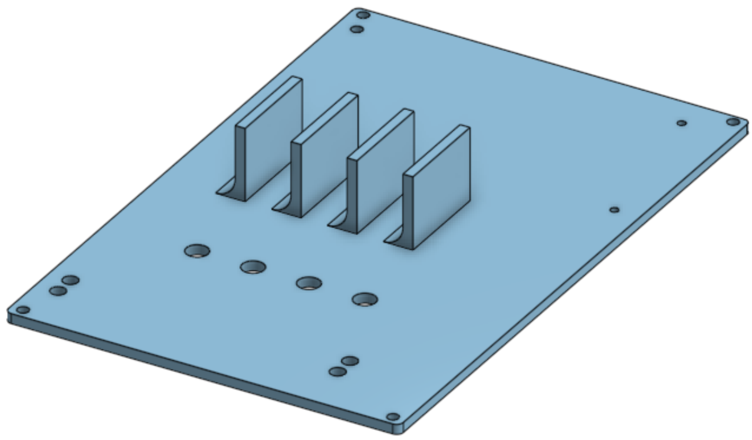

Figure 3.7: 3D printed piece for Control Model

The original design had to be modified to include connectors, electrical components, and wires in the box in order to meet the criteria needed for each of the components. Figure 3.8 shows a simplified layout of the control module after the modifications were made. The Cube Orange+, which powers the RTK-GPS by serial communication, is powered by a step-down converter connected to the 6S LiPo batteries. The RC Controller and the ODROID N2+ are powered by a second step-down converter that converts the 6S LiPo batteries' power from 8-35V to 12V 5A. Finally, the 4S LiPo batteries power the ESCs, which are connected to the thrusters themselves.

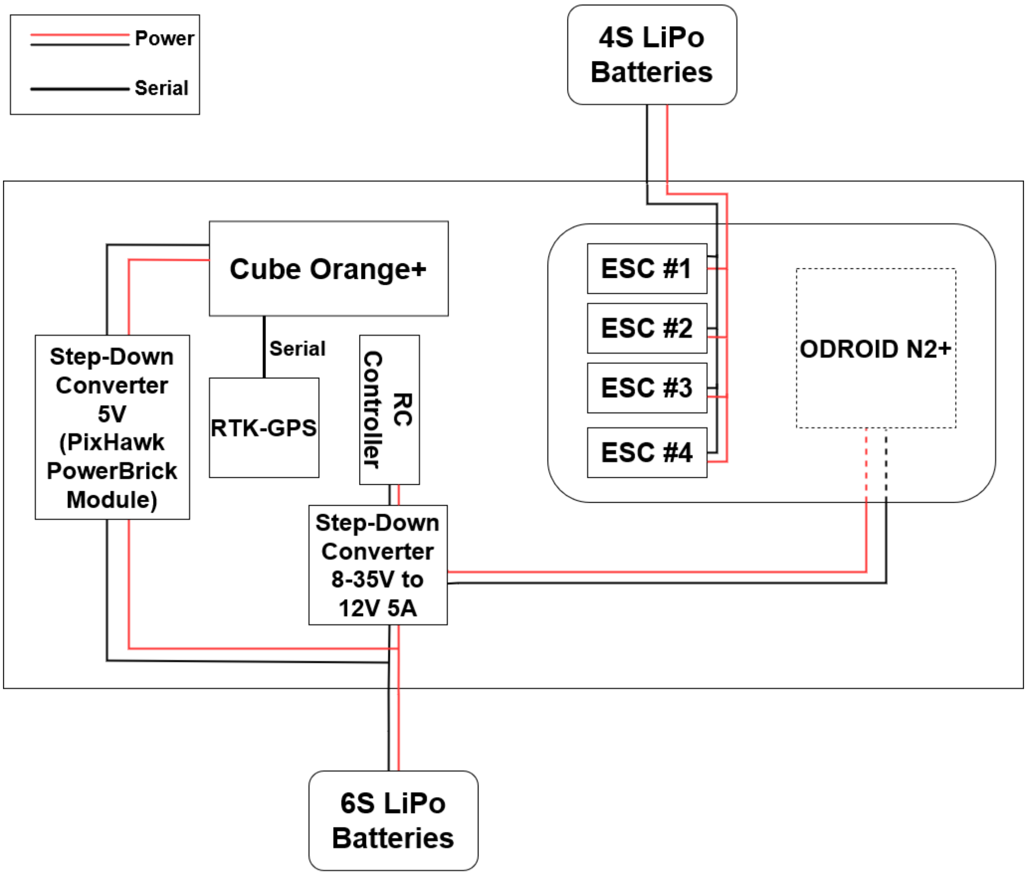

Figure 3.8: Hardware Layout of Control Module

Figure 3.9 illustrates how the thrusters were placed in strategic locations. These thrusters were specifically designed to have great omnidirectional thrust, enabling improved control and mobility in a variety of directions. Two clockwise (CW) and two counterclockwise (CCW) thrusters were arranged in the system's propulsion system, each of which improved the vehicle's overall stability and maneuverability. It should be noted that the two CW thrusters were installed at the rear of the vehicle, allowing for an effective backward drive, while the two CCW thrusters were mounted at the front, ensuring ideal forward propulsion.

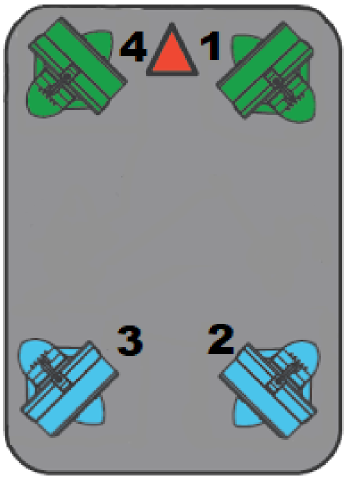

Figure 3.9: Thruster layout on NEST

Numerous wires and connectors that meet certain requirements had to be used since the control module had to be integrated with other parts and modules. Figure 3.10a shows the connectors and cables used to create the interface between the two modules, and figure 3.10b shows the design of the placement of these connectors and their respective cables. Each pair of cables and connectors is assigned a letter, for example, Cable A is mounted on the Connector A.

(a) Connectors and cables mounted on Control Module

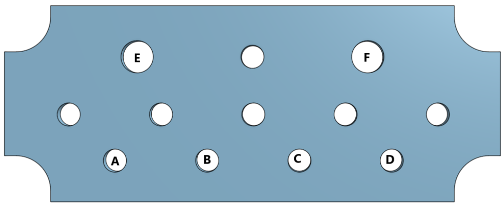

(b) Connectors placement design

Figure 3.10: Connectors placement

The requirements for the components used for the interface between the two modules, needed to ensure the material's protection, are shown in Table 3.2. The packages for the other components included all the additional cables and wires that were required but weren't on this list.

Finally, all of the parts and connectors were put together in the box to create the finished item that is depicted in Figure 3.11, where Figure 3.11a shows all of the parts put together in the box and Figure 3.11b shows the box with the connectors put in place.

Component	**Function**	**Requisites**
Box	Storage	IP Classification: IP68
Connector A	Power	IP Classification: IP68 Voltage: 16V Current: 20A
Connector B	Power	IP Classification: IP68 Voltage: 16V Current: 20A
Connector C	Power	IP Classification: IP68 Voltage: 16V Current: 20A
Connector D	Power	IP Classification: IP68 Voltage: 16V Current: 20A
Connector E	Power	IP Classification: IP68 Voltage: 16V Current: 25A per pin
Connector F	Power	IP Classification: IP68 Voltage: 24V Current: 25A per pin
Cable A	Power	IP Classification: IP68 Voltage: 16V Current: 20A
Cable B	Power	IP Classification: IP68 Voltage: 16V Current: 20A
Cable C	Power	IP Classification: IP68 Voltage: 16V Current: 20A
Cable D	Power	IP Classification: IP68 Voltage: 16V Current: 20A
Cable E	Power	IP Classification: IP68 Voltage: 16V Current: 25A per pin
Cable F	Power	IP Classification: IP68 Voltage: 24V Current: 25A per pin

Table 3.2: Requisites for the box, connectors and cables of the control module

All the parts and modules were put together on the NEST platform to complete the hardware, and the platform's functionality was then evaluated. NEST is depicted in Figure 3.12 with all the modules, wires, and parts placed into their respective locations. In the figure, the holding pad for the UAV was not present since it was being used for UAV perception tests, based on the detection of the ArTuga marker present on the landing pad [44].

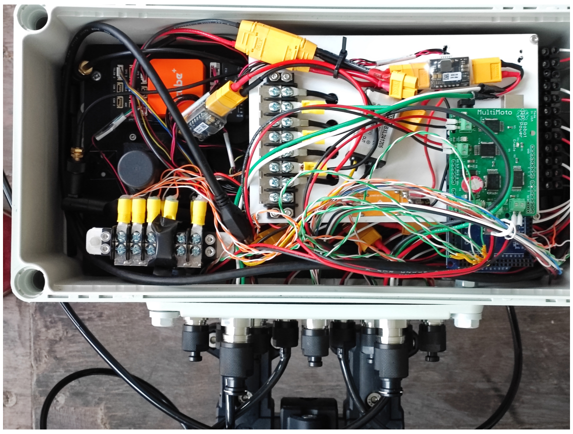

(a) Control Module fully assembled

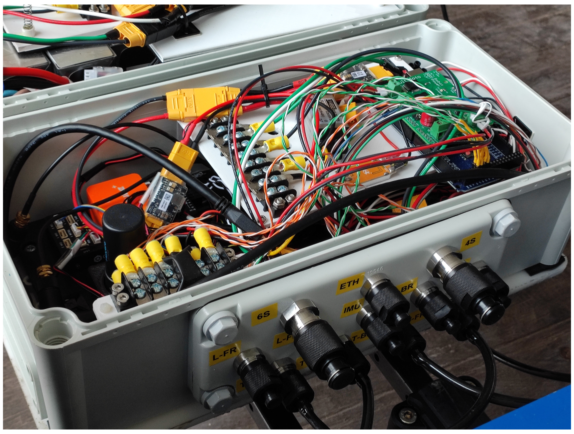

(b) Control Module's Connectors

Figure 3.11: Control Module Final Product

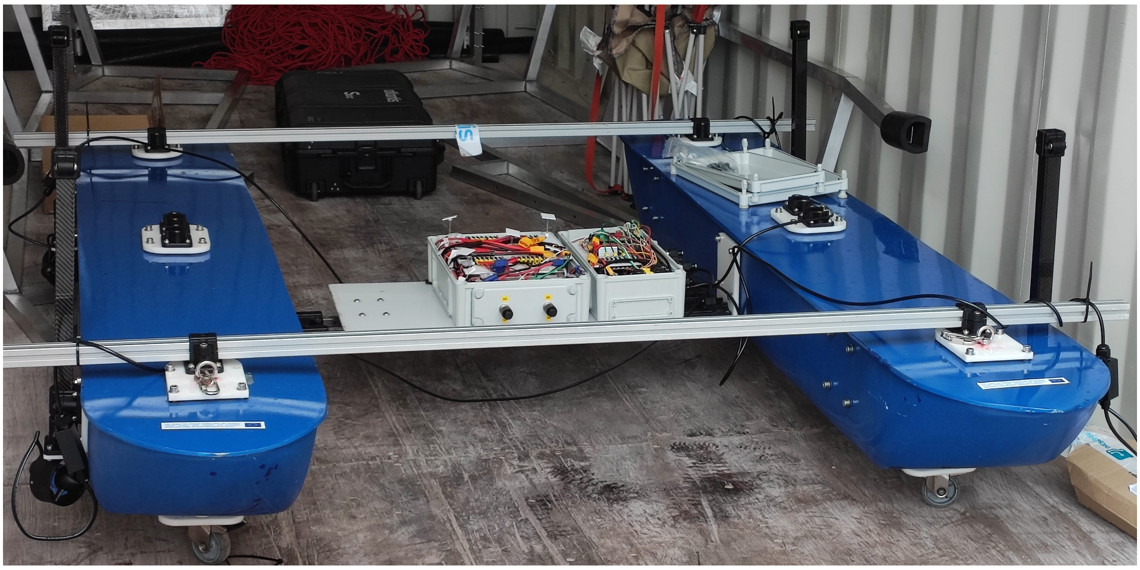

Figure 3.12: NEST platform fully assembled

3.2 Software Architecture

This dissertation aims to develop a real-time following system of an ASV by the NEST platform in a maritime scenario because there are not many of these systems with the necessary precision available and it fits within the scope of the project. The algorithm developed is a simple algorithm that allows the NEST to follow an ASV, enabling it to be autonomously transported by the ASV to the UAV's operation zone. The need for this algorithm is due to the fact that mechanical connections between NEST and ASV are to be avoided since they interfere with the maneuverability of the ASV with the inertia of the NEST-ASV platoon. The data collected by the system is obtained from this group of sensors:

- **IMU** (ICM42688): Sample rate: 10 Hz, Angular Precision: 0.0028º;
- **GPS** (Holybro F9P Helical): Sample rate: 20 Hz, Position Accuracy: 3D FIX-1.5 m/RTK-0.01 m;

With these sensors present on the NEST platform, the data obtained by each of these sensors is processed by the autopilot, providing the vessel's location, orientation, and speeds enabling the self-localization of the NEST platform.

In the next sections of this chapter, the methodology used for the algorithm developed, along with its results, as well as a description of the software that was provided by the autopilot, will be presented alongside the results of its implementation. The goal of the algorithm is to follow a point estimated by the current location of the vehicle that needs to be followed and make the platform follow it. The system has as its input the location data obtained by the sensors of the platform and the location data that the vessel to be followed provides, composed of odometry messages, providing us with position and velocity data. Figure 3.13 presents the flowchart of the different steps of the algorithm: point estimation and PID control. The inputs and outputs of each step are also present.

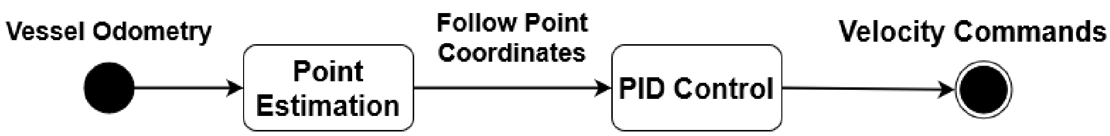

Figure 3.13: Overall flowchart of the developed algorithm

3.2.1 Position Estimation

This step of the algorithm has as its input the Vessel Odometry, with the data being published by the vessel to be followed. The output of this step is the coordinates of the point to be followed that were calculated through a series of mathematical and algebraic expressions. Figure 3.14 shows a leading ASV plotting several points that the NEST is able to follow.

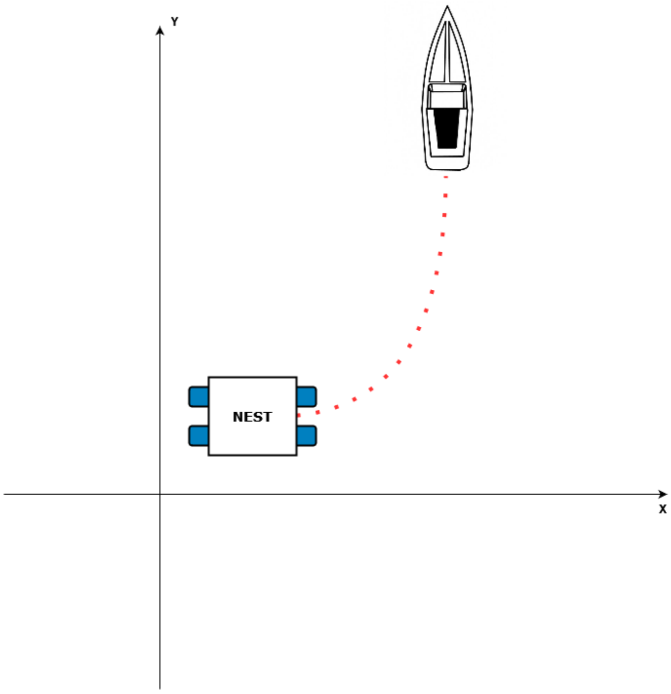

Figure 3.14: NEST Following various points defined by the ASV

Figure 3.15 presents the flowchart associated with this step of the algorithm.

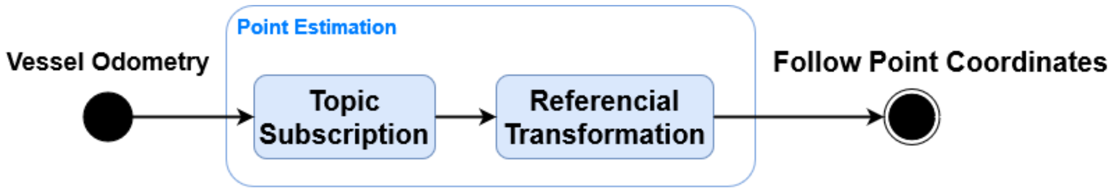

Figure 3.15: Flowchart of the developed algorithm in the Point Estimation step

The Vessel odometry is published as an odometry topic through Mavros[1]. The algorithm first subscribes to this topic to obtain the odometry data and then runs the necessary calculations and operations to obtain the position estimate coordinates. To subscribe to the topic, firstly a node handler is created so that it automatically manages the data that comes through that topic. Once the node handler is created, we subscribe to the topic of the Vessel Odometry and define a function callback where the data obtained through the topic is used to estimate the position estimate coordinates. The data obtained from the vessel is represented in the local frame of the vessel, and the point is in the global frame, as such the point must be passed to the local frame of the vessel. Figure 3.16 shows the schematics for the calculations of the position estimate coordinates.

The following sets of equations explain how to obtain the position estimate estimation, according to the frames shown in figure 3.16:

[1] https://ardupilot.org/dev/docs/ros.html

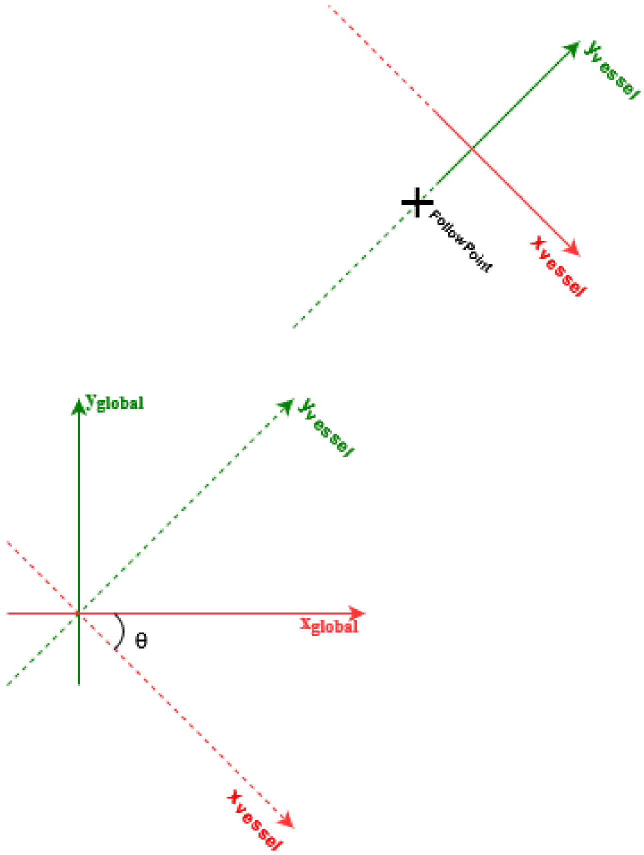

Figure 3.16: Schematics for calculations of position estimate coordinates

$$Point_x = x_{vessel} - (x_{offset}cos(\theta) - y_{offset}sin(\theta)) \tag{3.1}$$

$$Point_y = y_{vessel} - (x_{offset}sin(\theta) + y_{offset}cos(\theta)) \tag{3.2}$$

Equations 3.1 and 3.2 have as a result the coordinates in x and y since the Z axis is not relevant as the vessel will be working mainly in 2 dimensions (2D). $Point_x$ and $Point_y$ are the x and y coordinates of the position estimate, x_{offset} and y_{offset} are the offsets in the x-axis and y-axis, respectively, of the vessel frame to ensure that both vessels do not collide and θ is the angle between the axes of the vessel and global frame.

3.2.2 PID Control

Due to its simplicity, adaptability, and satisfactory performance in a wide range of applications, PID controllers were chosen to control the linear and angular speeds of the NEST platform and to enable the NEST to follow another vessel. Before starting the actual calculations, it is critical to initialize the PID controller. The PID controller then makes use of the position estimate coordinates to determine the optimal course of control action. The PID's speed instructions are transformed into high-quality commands that the platform can comprehend in the final step of this process. This transformation is essential to ensure that speed directives are in accordance with the particular requirements of the system in question.

Following the completion of the PID control step, speed instructions are generated that are essential for moving the vehicle and assisting it in achieving its goals. Figure 3.17 shows a flowchart that describes the essential steps and processes involved in this specific algorithmic level. This flowchart provides a comprehensive view of the interactions and activities that take place throughout the execution of the PID control.

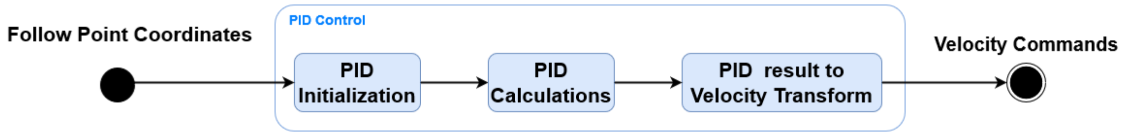

Figure 3.17: Flowchart of the developed algorithm in the PID Control step

To carry out the initialization of the PID Controller, it is necessary to create an object of the specific PID class. In the context of the algorithm in question, two objects of this class were created, one for the x-axis and another for the y-axis, in order to deal with the control in each of these dimensions. The fundamental arguments for the initialization of these objects are the proportional, integral, and derivative constants, which were previously determined using the manual PID adjustment method.

The values of the integral constant, K_i, and the derivative constant K_d are initially set to zero. Afterward, the proportional constant, K_p, is increased until the loop's output oscillates, and then it's reduced by about half for a more stable response. Afterward K_i is raised until any offset is fixed with enough time for the process, but not too high a value that results in instability. If necessary, K_d is raised until the loop can return to its reference after a load disturbance. Overshoot and excessive reaction are the results of too much K_d. In order to reach the setpoint more rapidly, a fast PID loop tuning typically overshoots significantly, nevertheless, some systems cannot accept overshoot, which calls for a K_p considerably lower than half of the oscillation-causing K_p level. Figure 3.18 shows how increasing each parameter of the PID has an effect on the overall process.

Through this manual adjustment method, the PID constants were carefully calculated, taking into account the specific characteristics and requirements of the system under study. These constants are fundamental to guarantee the proper performance of the PID controller, allowing it to respond accurately and efficiently to variations and deviations in the desired trajectory.

Parameter	Rise time	Overshoot	Settling time	Steady-state error	Stability
K_p	Decrease	Increase	Small change	Decrease	Degrade
K_i	Decrease	Increase	Increase	Eliminate	Degrade
K_d	Minor change	Decrease	Decrease	No effect in theory	Improve if K_d small

Figure 3.18: Effects of increasing a parameter independently [45].

The PID controller's implementation, together with its calculation process and variable settings, is shown in the code snippet below.

```
class PID{
public:
  double kp, ki, kd;
  //kp constant influences the proportional aspect
  //ki constant influences the integral aspect
  //kd constant influences the derivative aspect


  double calculate(double target, double measure){

    error = target - measure;

    //Integral aspect is the sum of all errors obtained in the loop
    integral += error;

    //Anti-windup mechanism

    if (integral > 25){
        integral = 25;
    }
    else if (integral < -25){
        integral = -25;
    }


    //Derivative aspect is the difference between current error and last error
    derivative = error - previousError;

    //The output is the sum of all aspects multiplied by their corresponding constants
    output = kp * error + ki * integral - kd * derivative;
```

```
    previousError = error;

    //Returns the output
    return output;
  }

private:
  double error,integral,derivative,output,previousError;
  //Here the value of each calculated value is stored privately
};
```

The intended value, which corresponds to the position estimate coordinates, and the current measure, which comprises the current location on the x and y axes of the NEST platform, are used by the PID Controller to execute computations after the initialization stage. Once the PID has gotten the results for each axis, these results must be transformed in order to provide speeds that the platform can comprehend. When performing this transformation, a series of equations are employed to make sure the resulting velocities are expressed properly and coherently so they can be later published and transmitted to the actuators in charge of moving the platform.

This process of transforming the PID results is critical to ensure efficient and responsive motion control, allowing the platform to accurately follow the desired trajectory in response to variations in the position estimate coordinates. The equations that were used in this transformation process are shown below:

$$yaw = \theta_{NEST} - \pi/2, with - \pi < yaw < \pi \tag{3.3}$$

$$\theta_R = atan2(sin(\theta_{vessel}), cos(\theta_{vessel})) - atan2(sin(yaw), cos(yaw)), with - \pi < \theta_R < \pi \tag{3.4}$$

$$V_x = PID_X cos(yaw) + PID_Y sin(yaw) \tag{3.5}$$

$$V_y = PID_X(-sin(yaw)) + PID_Y cos(yaw) \tag{3.6}$$

The angle of the NEST platform in relation is depicted by θ_{NEST} in relation to the world frame, and since this angle has an offset of $pi/2$ radians, the *yaw* describes the correct angle of the NEST platform. θ_R depicts the angle between the NEST and the leading vessel, V_x and V_y depict the velocities calculated with the values obtained from the PID controller, PID_X being the result of the PID in the x-axis and PID_Y being the result of the PID in the y-axis.

3.2.3 Navigation Profiles

In the realm of hardware components, certain integral elements, such as the autopilot, are endowed with advanced software features that greatly enhance their functionalities. Notably, among these built-in software capabilities are the remarkable station-keeping and go-to functionalities. To assess the effectiveness and reliability of the software bundled with this specific equipment, rigorous testing was conducted in Viana do Castelo, Portugal, without introducing any modifications to the original software configuration. Concurrently with the hardware testing, comprehensive evaluations were performed to validate the performance and robustness of the associated software.

One notable software feature, known as the waypoint navigation mode, allows one to designate a precise location on the map to which the vessel is intended to navigate. Once the destination is specified, the vessel autonomously undertakes the entire journey, effectively demonstrating its autonomous navigation capabilities. Moreover, in instances where the objective is to maintain the vessel's position in a particular area for an extended duration, a mode commonly referred to as loiter mode or station-keeping can be engaged. This mode enables the vessel to attain a stable and controlled position on the designated map location, thereby facilitating various tasks or operations conducted within that specific geographical vicinity.

In addition, another relevant functionality, which involves the waypoint navigation capability, was employed. Through mission planning, it became possible to establish multiple points on the map, which allows the vehicle, through a combination of waypoint navigation procedures, to trace more complex routes. This mission planning capability makes it possible to create customized and adaptable routes, considering a variety of destinations along the way. By defining these points on the map, the vehicle is able to navigate autonomously, accurately, and reliably following the predetermined path.

These features improve the platform's behavior and adaptability in addition to the algorithm created for this thesis, enabling it to carry out more difficult operations.

Chapter 4

Results Analysis

4.1 Introduction

The NEST concept allows UAVs to land on their landing pad. Its innovative features are the ability to perform station-keeping, waypoint navigation, mission planning, and vessel following. In terms of hardware and autonomous navigation, the results of the validation of NEST's resilience and dependability will be presented in this chapter. The tests that were carried out for this chapter included validation in real situations like the ATLANTIS Coastal Testbed in Viana do Castelo, Portugal, and simulation engines like Gazebo. All of the system's intrinsic functionality, including station-keeping, waypoint navigation, mission planning, and vessel following, are validated by these tests.

4.2 Simulated Results

To test the developed algorithm and the systems' other available functionalities, the Gazebo simulator was used allowing the simulation of a dynamic maritime environment, capable of simulating currents, winds, and waves. This ability to simulate real-life behaviors allows for a greater approximation of the simulation with the tests performed in a live scenario.

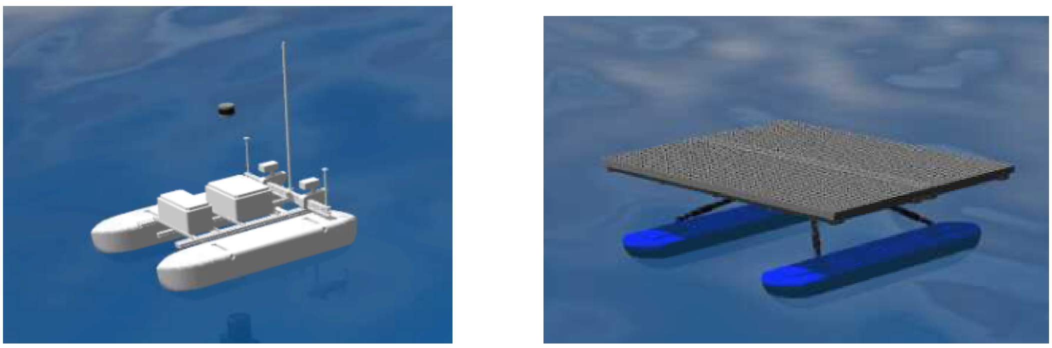

(a) SENSE ASV representative model (b) NEST platform representative model

Figure 4.1: Representative models of SENSE ASV and NEST platform in Gazebo simulator

As shown in figure 4.2, the position estimate is accurate, due to the fact that the position estimate has an offset in the x-axis of the vessel frame of value 5m, and as seen in the final point the difference in the x-axis between the vessel position and the position estimate coordinates is exactly 5 meters.

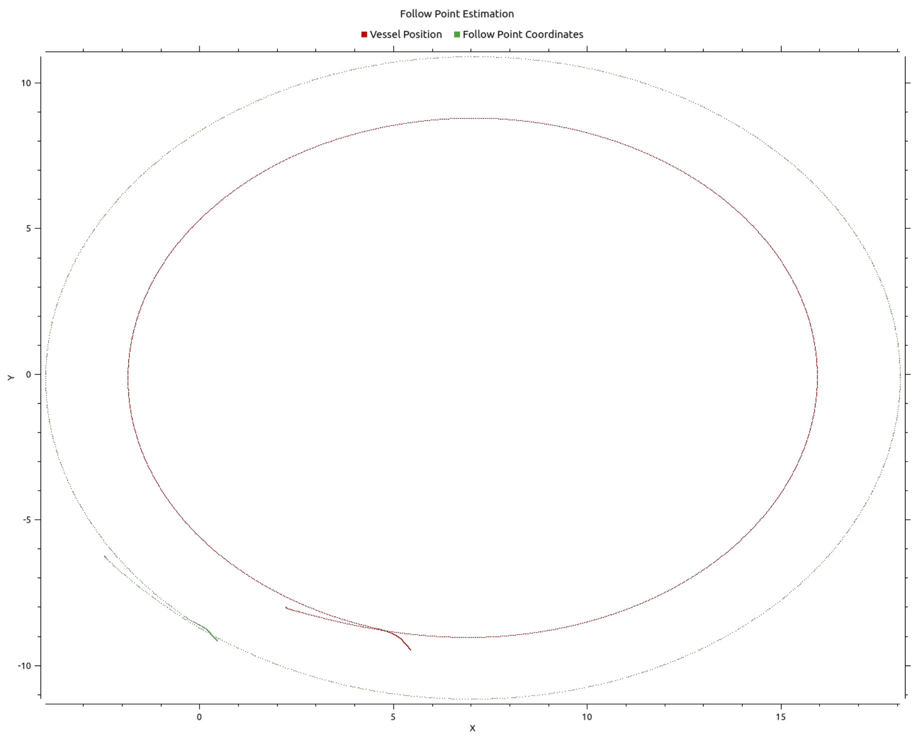

Figure 4.2: Position estimate coordinates with vessel position with a circular trajectory

The same position estimate is depicted in Figure 4.3 but with a different trajectory. Because the position estimate coordinates depend on the vessel's orientation, occasionally inconsistent results can happen. For instance, although the distance between the two vessels in the above figure is exactly 5 m, it appears to be greater due to the vessel's orientation with respect to the x-axis, which requires that the coordinates of the position estimate be adjusted in order to maintain the intended distance between the two vessels.

After the Point Estimation, the position estimate coordinates are sent through a PID controller, where the measured value is the current location of the NEST platform and the desired value is the coordinates of the position estimate. In Figure 4.4, a visual representation of the PID response to a sudden change in the required values is presented, thereby offering a clear depiction of the system's dynamic behavior.

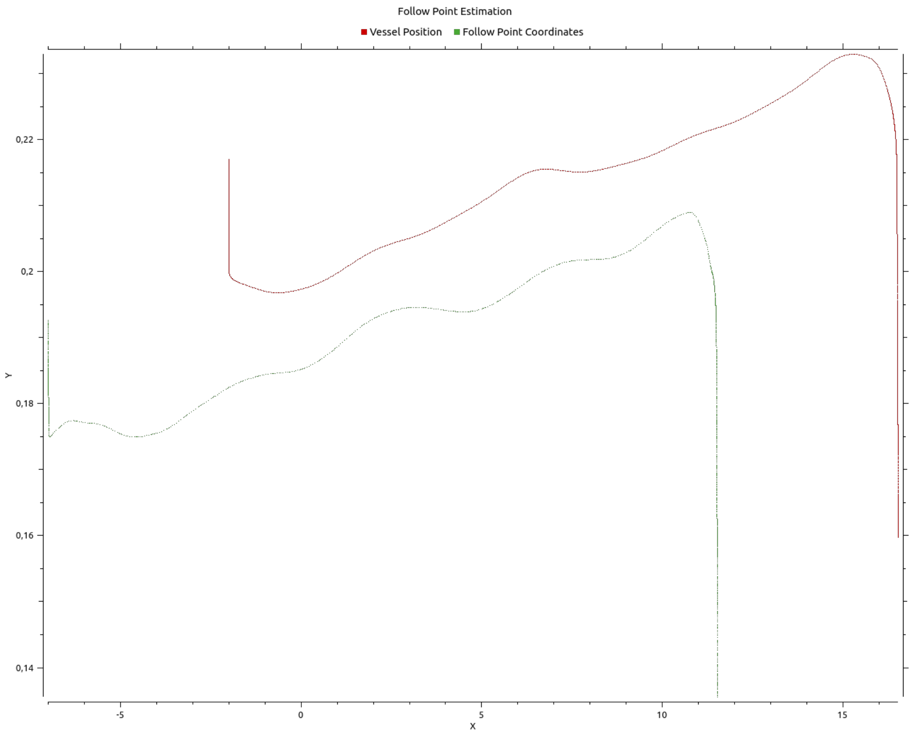

Figure 4.3: Position estimate coordinates with vessel position with an irregular trajectory

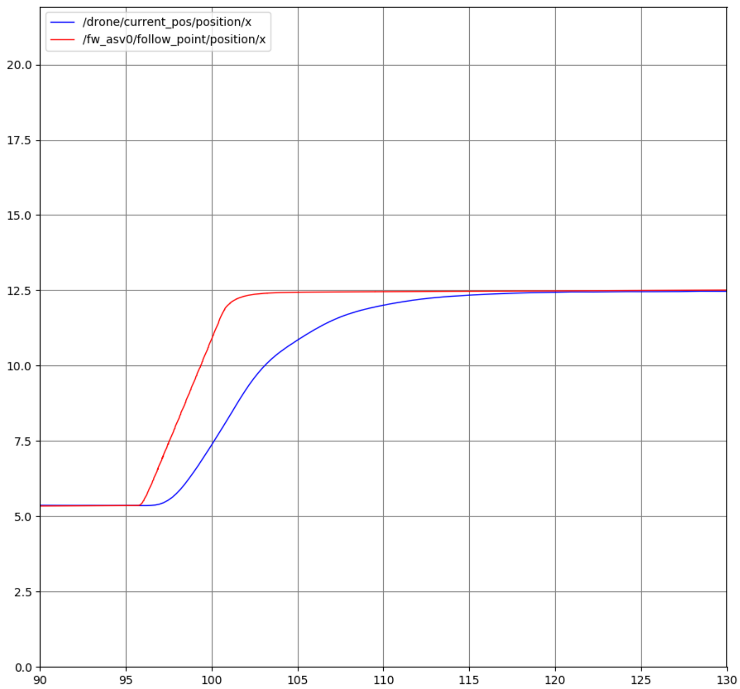

Figure 4.4: PID response to a sudden change in position
(red is the desired position and blue is the current measurement)

The observed response exhibits good characteristics, notably the system's promptness and stability in adapting to the abrupt alteration in the desired values. This performance is accomplished without giving in to the unfavorable wind-up or overshoot phenomena, which are frequently linked to ineffective control systems. The absence of wind-up signifies that the system successfully avoids excessive integral accumulation, thereby preventing prolonged oscillations or undue overshooting of the setpoint. Moreover, the absence of overshoot further underscores the system's dependability by ensuring that it accurately tracks and attains the desired values without overshooting or exceeding the target. The behavior exhibited by the system in this experiment reinforces its reliability and robustness.

The reliability of the system was assessed by conducting tests using the Gazebo simulation engine. The system underwent rigorous testing across various scenarios, encompassing varying intensities of currents, winds, and waves. Strong currents were applied to the Gazebo simulator in order to further test the PID control by complicating the movement of the NEST platform and observing how the system responded to these unfavorable conditions. This was tested in four different settings, each of which is shown in figure 4.5:

- Positive Current speeds in the x-axis of the global frame.
- Positive Current speeds in the y-axis of the global frame.
- Negative Current speeds in the x-axis of the global frame.
- Negative Current speeds in the y-axis of the global frame.

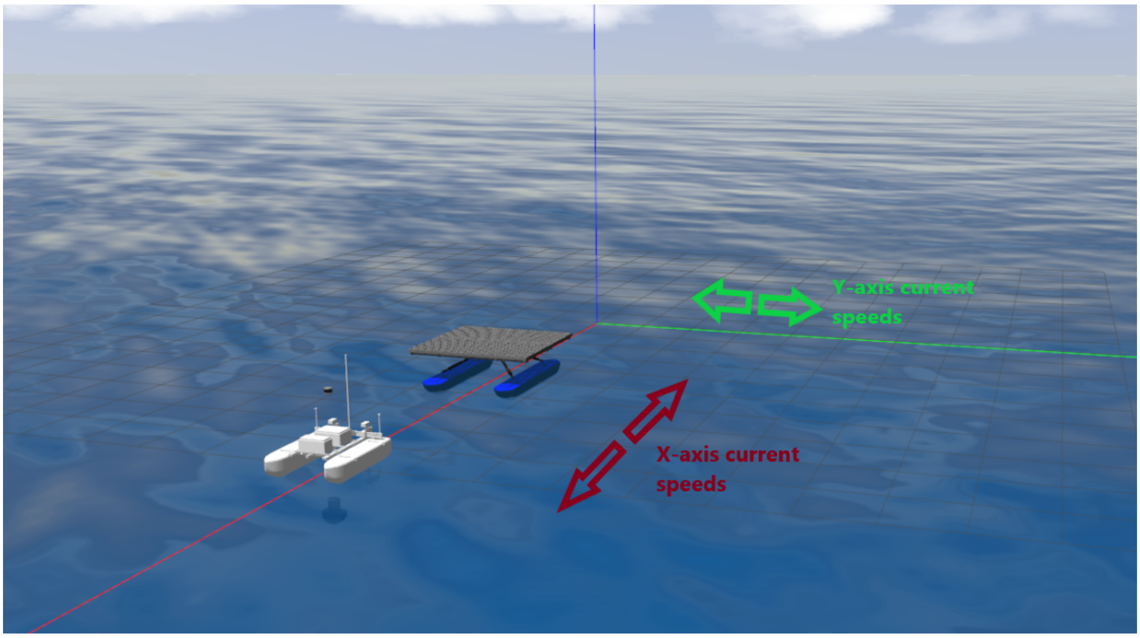

Figure 4.5: Gazebo reliability test scenario

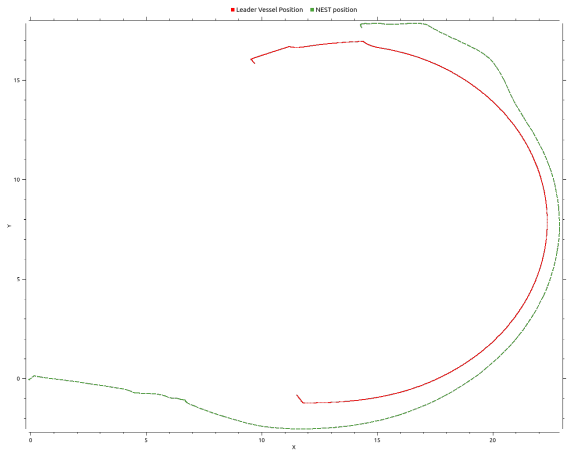

(a) Positive x-axis Current speed

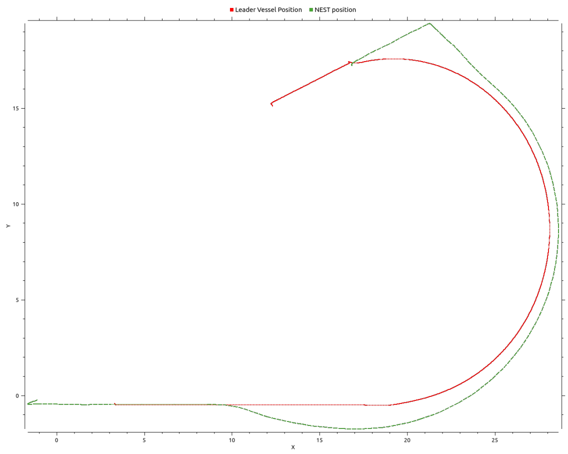

(b) Positive y-axis Current speed

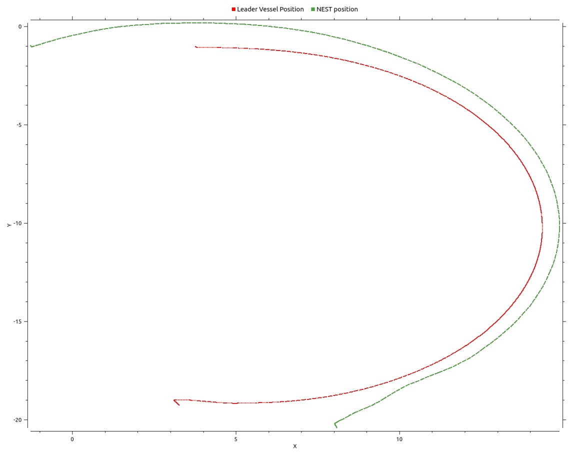

(c) Negative x-axis Current speed

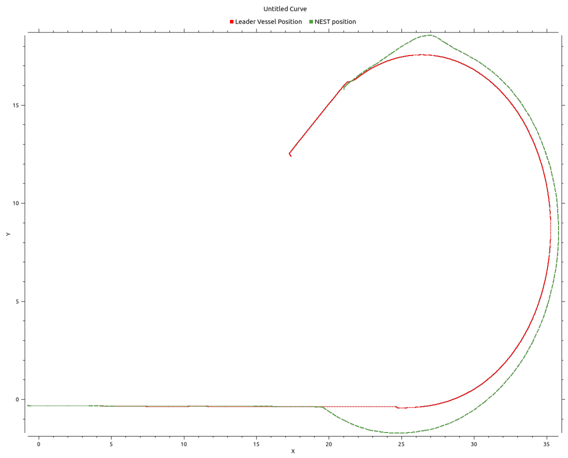

(d) Negative x-axis Current speed

Figure 4.6: Vessel following trajectory with different current speeds
(red is the leading vessel and green is the NEST platform)

As depicted in figure 4.6, the system exhibits the ability to diligently track and follow the leading vessel with remarkable precision, even in the face of challenging environmental factors such as strong currents. This noteworthy performance not only validates the accurate and effective computation of the PID Controller but also serves as a tangible confirmation that it seamlessly operates in real-time, precisely meeting the expected performance standards. Figures 4.7 and 4.8 show that the developed algorithm performs more reliably and smoothly than the HLOS-based approach, which is covered in section 2.2. The key difference between the two is the use of obstacle avoidance, which the constructed algorithm does not use. Due to the technique's high simulation accuracy and dependability, it can be employed in real-world applications.

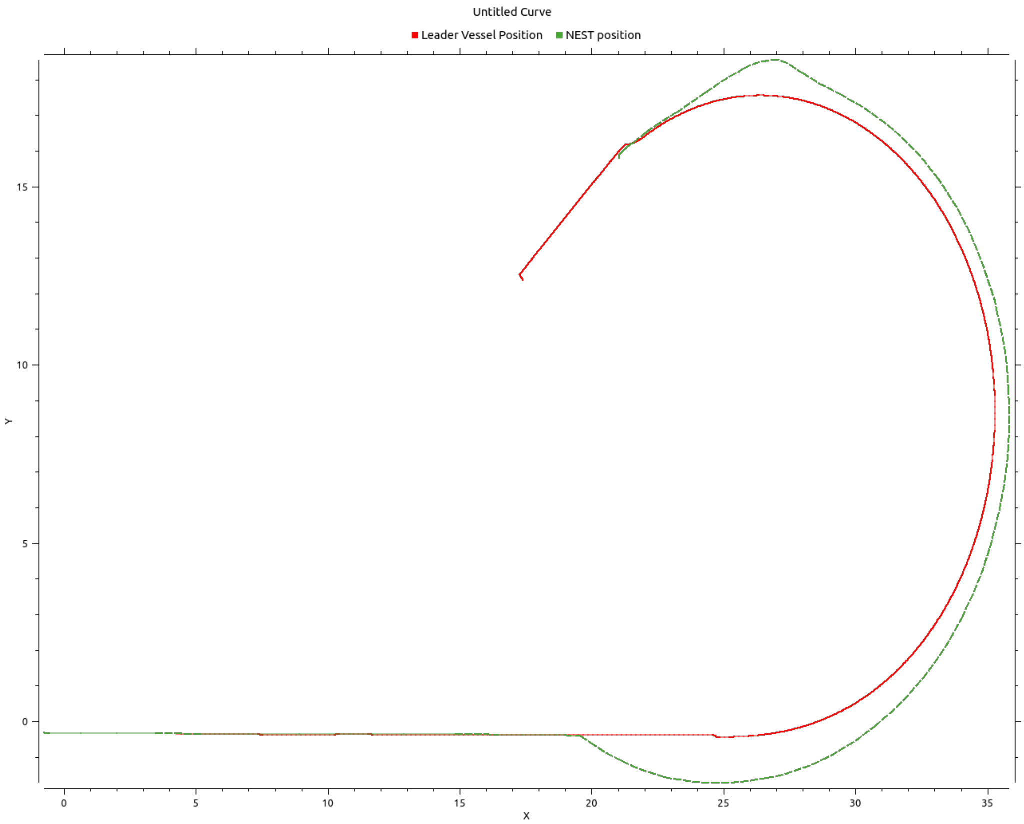

Figure 4.7: Developed Method
(Red is the ASV position and green is the NEST position)

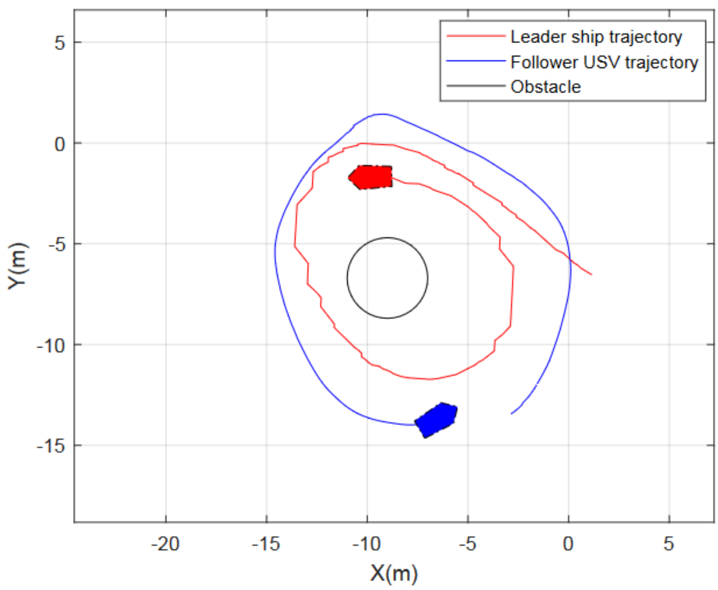

Figure 4.8: HLOS-based method [11]

4.3 Live Results

To thoroughly evaluate the full range of capabilities offered by the system, a meticulously planned and executed series of rigorous tests took place within the coastal testbed of Viana do Castelo. These tests were designed with the primary objective of acquiring insights into the autonomous navigation capabilities of the NEST. Moreover, they sought to assess and gauge the performance and efficiency of its hardware components, ensuring a thorough understanding of the system's overall functionality and operational effectiveness.

The first test that was conducted was the hardware test, where the performance of the thrusters, the efficiency of the batteries, and the responsiveness of the platform were evaluated. These tests were conducted with unfavorable sea conditions, namely strong currents however, the NEST was able to perform exceptionally well under these conditions, demonstrating great speeds when moving in any direction and rotation. The power efficiency was also proven to be quite high since in a 75-minute mission the 6S dropped only 5% of their total value and the 4S batteries dropped to 40% of their total value. The tests that were conducted can be shown here[1]. After these hardware tests were conducted, the autonomous navigation features were tested, beginning with the station-keeping procedure.

Figure 4.9: NEST in Coastal Testbed

[1] https://youtu.be/TQkvh0FWoJI

The station-keeping procedure, also known as loiter mode, was the first autonomous navigation procedure to be tested. The NEST was given instructions to loiter as near as possible to a designated loiter site. The position of the NEST and the specified point are shown in red and green, respectively, in Figure 4.12. The platform starts moving toward the target position early on, which is why a straight line is displayed between $x = 0.4m$ and $x = 0.8m$. The platform deviates somewhat from the desired spot when it is in position because of the impacts of the wave and current. The maximum variation over a 2-minute long operation for x is 0.35 meters and y is 0.4 meters. The NEST has a mean deviation in the x-axis of 0.022 m and in the y-axis of 0.02627 m. The mean distance deviation to the loiter point is 0.034318m. It is possible to watch a video of this process being tried here[2].

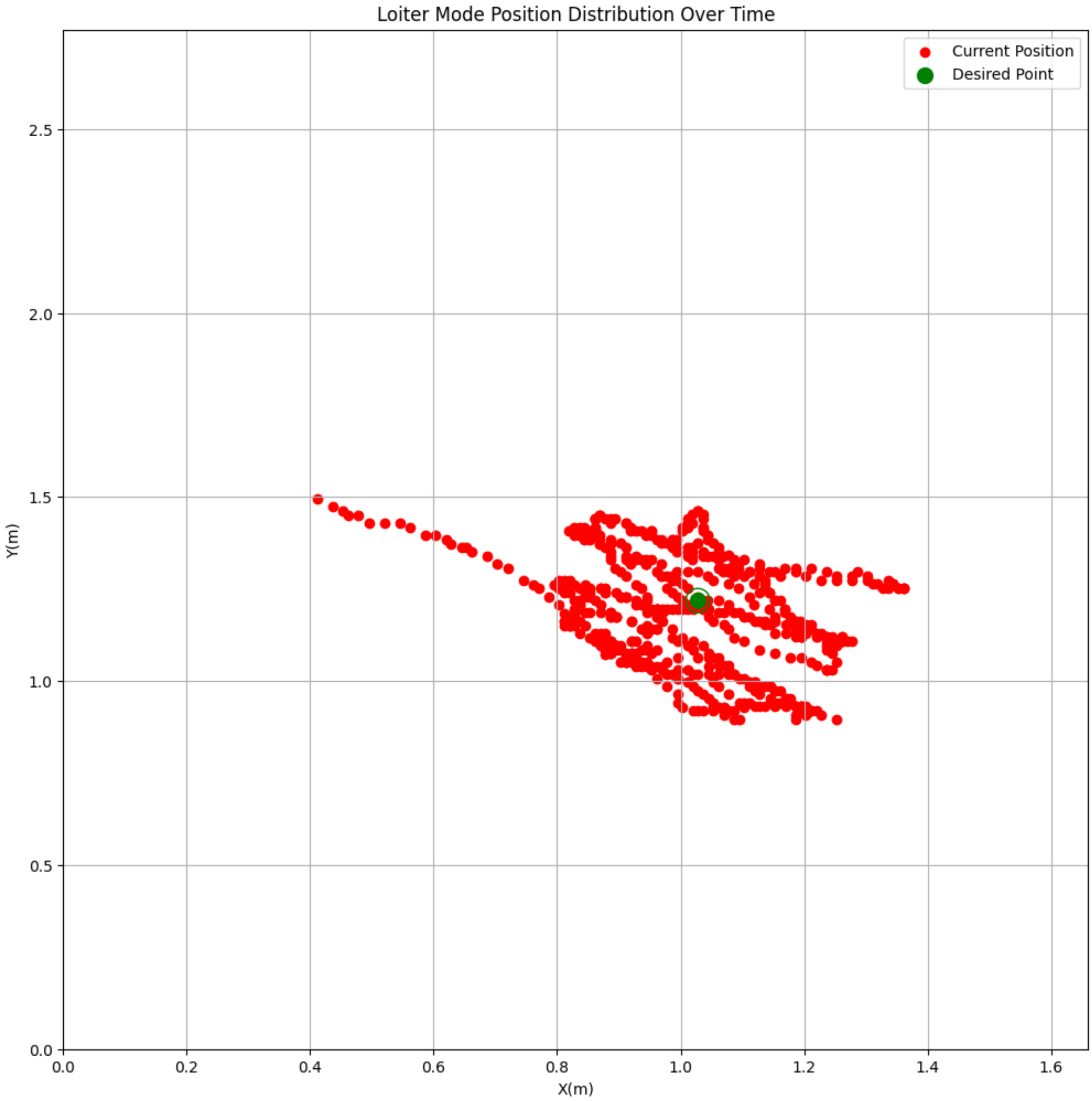

Figure 4.10: Station-Keeping results in maritime scenario

[2] https://youtube.com/shorts/f913F395ygQ

Figure 4.11: Coastal Testbed Station-keeping

Waypoint navigation, or Guided mode, was tested next after the Loiter Mode. The trajectory of the NEST is depicted in Figure 4.12 along with the NEST's initial position, desired position, and the best route between these three sites. As shown, the NEST's trajectory does not initially follow the ideal path because the software interprets its dynamics as differential when, in fact, the NEST has omnidirectional dynamics and is capable of rotating on its own axis and moving in all directions. The software gives the left-side thrusters greater power since it assumes differential dynamics and the platform is 90 degrees from its final position; as a result, the platform rotates and moves at the same time, producing the curving line from $x = 0.0m$ to $x = 7.5m$, obtaining a maximum deviation from the ideal path of 2.94m. Once the perfect orientation has been attained, the NEST's trajectory will follow the ideal path with a maximum deviation of 1.12 meters. Furthermore, the NEST is able to complete this trajectory in a short amount of time of 29.819861 seconds. The mean deviation on the x-axis is 1.2958 m and on the y-axis is 0.2524m, with a mean distance deviation to the ideal path of 1.3201m. A video demonstrating the waypoint navigation process can be shown here[3].

[3] https://youtube.com/shorts/z5mayVxmQhI

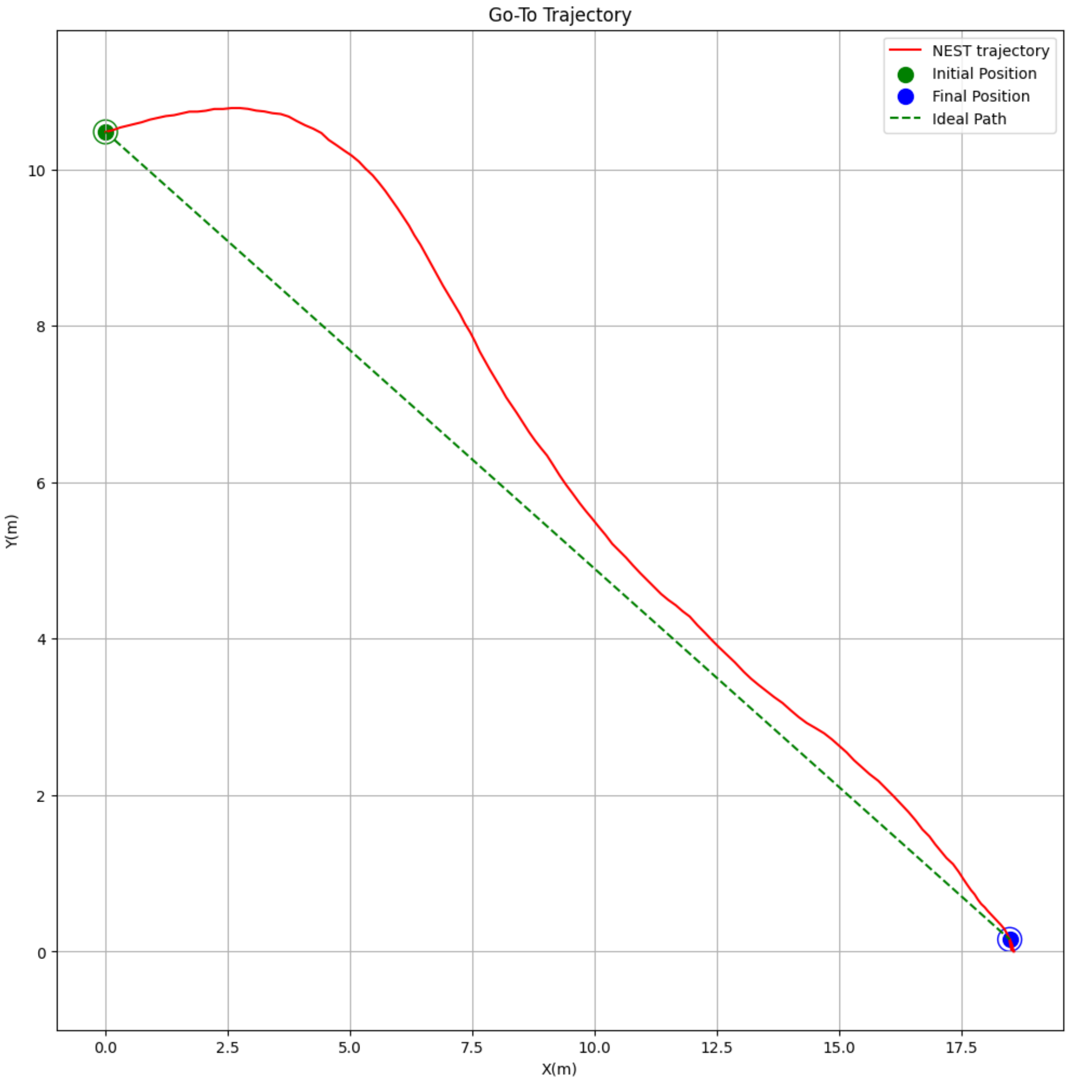

Figure 4.12: Guided Mode results in maritime scenario

The Mission Mode was the last mode to be tested. In this mode, several waypoints are defined for the platform to travel to and different waypoint navigation techniques are used to get there. The defined sequential waypoints are shown in yellow in Figure 4.13, and the NEST's trajectory and current position are shown in red and yellow, respectively. Although the NEST successfully followed the ideal path between each pair of points throughout the mission; deviations, with a maximum deviation of 1.5m, occurred during turning maneuvers because the software assumed the NEST operates as a differential drive vessel, thereby affecting its path accuracy. The total operation time of this test was 3 minutes, accumulating a mean deviation error on the x-axis of 1.7253 m and on the y-axis of 0.3152m, with a mean distance deviation to the ideal path of 1.7539m during the course of this test.

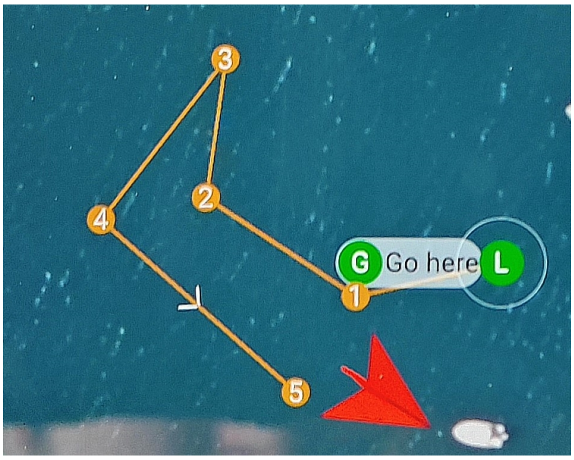

(a) Defined Waypoints

(b) NEST Trajectory

Figure 4.13: Mission Results

In conclusion, the outcomes of the tests and assessments that were performed provided helpful information about how well the NEST platform's features functioned. Although each feature has certain variations, it has become clear that the platform is capable of traveling to different positions, navigating between different designated points, and maintaining its current position.

Chapter 5

Conclusions and Future Work

With the maintenance of offshore wind farms being of difficult access and quite expensive, the use of ASVs to this effect presents an important solution. By allowing cooperation between various vessels, the efficiency of the process will increase significantly and allow for safer and more reliable sustainability of these structures. However to ensure, the safety of the process and the integrity of each component and vessel involved, the need to develop reliable real-time algorithms. As such, this thesis revolves around these systems, obtaining a platooning method with additional capabilities with high precision and responsiveness. This algorithm is based on communication between vessels, and for this effect, the communication methods must be reliable and responsive. The vessels provide each other with their current positions, through the use of various sensors, such as GPS and IMU. Initially, the algorithm receives the Vessel Odometry from the leader vessel and transforms the data so that the algorithm can understand it. The next step is PID Control, in which we pass the data obtained through a PID, which calculates the output that needs to be applied in each axis according to the current and desired position. Finally, the output result in transformed into velocity commands so that the actuators can perceive the command and act accordingly. This algorithm was tested only in simulation as such, some future work includes testing in a maritime scenario. Although the algorithm possesses a high level of precision, there are recurrent technological advancements that allow for better results. As such, exploring other approaches or using another point of view is beneficial to any scientific work. To be capable of testing the system in a real environment, the system was mounted on a physical vessel with electronic and mechanical systems. Although the system is functional and safe to operate, there are always aspects to improve the efficiency or overall safety of the structure. Furthermore, when testing at seashore the algorithm failed to work since the vessels failed to communicate with each other due to weak wireless signals. As such, to counteract this problem some additional work needs to be done so that the system can function without issues. This future work includes:

- Improve Mechanical aspects of the structure, for example, sturdier mechanical components.
- Improve Electrical aspects of the system, for example, better wiring arrangements and better communication modules.

References

[1] International Renewable Energy Agency. *RENEWABLE ENERGY STATISTICS 2022 STATISTIQUES D'ÉNERGIE RENOUVELABLE 2022 ESTADÍSTICAS DE ENERGÍA RENOVABLE 2022 About IRENA*. 2022. URL: https://www.irena.org/publications/2022/Jul/Renewable-Energy-Statistics-2022.

[2] O. Khalid, G. Hao, C. Desmond, et al. Applications of robotics in floating offshore wind farm operations and maintenance: Literature review and trends. *Wind Energy*, 25(11):1880–1899, 2022. doi:https://doi.org/10.1002/we.2773.

[3] Khristopher Kabbabe Poleo, William J. Crowther, and Mike Barnes. Estimating the impact of drone-based inspection on the levelised cost of electricity for offshore wind farms. *Results in Engineering*, 9:100201, 2021. doi:https://doi.org/10.1016/j.rineng.2021.100201.

[4] Xiaohua Ge, Qing-Long Han, Qing Wu, and Xian-Ming Zhang. Resilient and safe platooning control of connected automated vehicles against intermittent denial-of-service attacks. *IEEE/CAA Journal of Automatica Sinica*, 10(5):1234–1251, 2023. doi:10.1109/JAS.2022.105845.

[5] Yifeng Han, Tomoya Kawasaki, and Shinya Hanaoka. The benefits of truck platooning with an increasing market penetration: A case study in japan. *Sustainability*, 14(15), 2022. doi:https://doi.org/10.3390/su14159351.

[6] J. Scholl, N. Boysen, and A. Scholl. E-platooning: Optimizing platoon formation for long-haul transportation with electric commercial vehicles. *European Journal of Operational Research*, pages 525 – 42, 2023//. doi:http://dx.doi.org/10.1016/j.ejor.2022.04.013.

[7] Minhyeong Lee and Dongjun Lee. A distributed two-layer framework for teleoperated platooning of fixed-wing uavs via decomposition and backstepping. *IEEE Robotics and Automation Letters*, 6(2):3655–3662, 2021. doi:10.1109/LRA.2021.3064207.

[8] N. Pourmohammad-Zia, F. Schulte, and R.R. Negenborn. Platform-based platooning to connect two autonomous vehicle areas. pages 6 pp. –, Piscataway, NJ, USA, 2020//. doi:http://dx.doi.org/10.1109/ITSC45102.2020.9294689.

[9] DooYong Oh, Hoon Je Woo, and Jung Ha Kim. The research of dynamic network architecture for platooning ugvs. In *ICCAS 2010*, pages 1105–1108, 2010. doi:10.1109/ICCAS.2010.5669726.

[10] Dominik Juling. Truck platooning. *The RUSI Journal*, 0(0):1–8, 2023. doi:10.1080/03071847.2023.2195897.

[11] Bin Du, Bin Lin, Wei Xie, Weidong Zhang, Rudy R. Negenborn, and Yusong Pang. Flexible collision-free platooning method for unmanned surface vehicle with experimental validations. In *2022 IEEE/RSJ International Conference on Intelligent Robots and Systems (IROS)*, pages 6854–6860, 2022. doi:10.1109/IROS47612.2022.9981043.

[12] Yunsheng Fan, Jianlei Ma, Guofeng Wang, and Tieshan Li. Design of a heterogeneous marsupial robotic system composed of an usv and an uav. pages 395–399. IEEE, 2 2016. doi:10.1109/ICACI.2016.7449858.

[13] R.R. Murphy. Marsupial and shape-shifting robots for urban search and rescue. *IEEE Intelligent Systems*, 15:14–19, 3 2000. doi:10.1109/5254.850822.

[14] Michail Kalaitzakis, Brennan Cain, Nikolaos Vitzilaios, Ioannis Rekleitis, and Jason Moulton. A marsupial robotic system for surveying and inspection of freshwater ecosystems. *Journal of Field Robotics*, 38(1):121–138, 2021. doi:https://doi.org/10.1002/rob.21957.

[15] Eduardo Pinto, Francisco Marques, Ricardo Mendonça, André Lourenço, Pedro Santana, and J. Barata. An autonomous surface-aerial marsupial robotic team for riverine environmental monitoring: Benefiting from coordinated aerial, underwater, and surface level perception. 12 2014. doi:10.1109/ROBIO.2014.7090371.

[16] Andry Maykol Pinto, Joao V. Amorim Marques, Daniel Filipe Campos, Nuno Abreu, Anibal Matos, Martio Jussi, Robin Berglund, Jari Halme, Petri Tikka, Joao Formiga, Christian Verrecchia, Serena Langiano, Clara Santos, Nuno Sa, Jaap-Jan Stoker, Fabrice Calderoni, Shashank Govindaraj, Alexandru But, Leslie Gale, David Ribas, Natalia Hurtos, Eduard Vidal, Pere Ridao, Patryk Chieslak, Narcis Palomeras, Stefano Barberis, and Luca Aceto. Atlantis - the atlantic testing platform for maritime robotics. pages 1–5. IEEE, 9 2021. doi:10.23919/OCEANS44145.2021.9706059.

[17] Rafael Marques Claro, Diogo Brandão Silva, and Andry Maykol Pinto. Artuga: A novel multimodal fiducial marker for aerial robotics. *Robotics and Autonomous Systems*, 163:104398, 5 2023. doi:10.1016/j.robot.2023.104398.

[18] Seong-Woo Kim, Wei Liu, Marcelo H. Ang, Emilio Frazzoli, and Daniela Rus. The impact of cooperative perception on decision making and planning of autonomous vehicles. *IEEE Intelligent Transportation Systems Magazine*, 7:39–50, 2015. doi:10.1109/MITS.2015.2409883.

[19] Muhammad Abu Bakr and Sukhan Lee. Distributed multisensor data fusion under unknown correlation and data inconsistency. *Sensors*, 17:2472, 10 2017. doi:10.3390/s17112472.

[20] Jianhua Wang, Wei Gu, Jianxin Zhu, and Jubiao Zhang. An unmanned surface vehicle for multi-mission applications. pages 358–361. IEEE, 2 2009. doi:10.1109/ICECT.2009.136.

[21] Anibal Matos, Alfredo Martins, Andre Dias, Bruno Ferreira, Jose Miguel Almeida, Hugo Ferreira, Guilherme Amaral, Andre Figueiredo, Rui Almeida, and Filipe Silva. Multiple robot operations for maritime search and rescue in eurathlon 2015 competition. pages 1–7. IEEE, 4 2016. doi:10.1109/OCEANSAP.2016.7485707.

[22] Waleed Al Maawali, Ahmed Al Naabi, Majid Al Yaruubi, Ashraf Saleem, and Ahmed Al Maashri. Design and implementation of an unmanned surface vehicle for oil spill handling. pages 1–6. IEEE, 2 2019. doi:10.1109/UVS.2019.8658267.

[23] Daniel Filipe Campos, Aníbal Matos, and Andry Maykol Pinto. Modular multi-domain aware autonomous surface vehicle for inspection. *IEEE Access*, 10:113355–113375, 2022. doi:10.1109/ACCESS.2022.3217504.

[24] Maria Inês Pereira, Rafael Marques Claro, Pedro Nuno Leite, and Andry Maykol Pinto. Advancing autonomous surface vehicles: A 3d perception system for the recognition and assessment of docking-based structures. *IEEE Access*, 9:53030–53045, 2021. doi:10.1109/ACCESS.2021.3070694.

[25] Maria Inês Pereira, Pedro Nuno Leite, and Andry Maykol Pinto. Detecting docking-based structures for persistent asvs using a volumetric neural network. In *Global Oceans 2020: Singapore – U.S. Gulf Coast*, pages 1–6, 2020. doi:10.1109/IEEECONF38699.2020.9389349.

[26] Rafael Claro, Renato Silva, and Andry Pinto. Detection and mapping of monopiles in offshore wind farms using autonomous surface vehicles. In *Global Oceans 2020: Singapore – U.S. Gulf Coast*, pages 1–4, 2020. doi:10.1109/IEEECONF38699.2020.9389348.

[27] Daniel Filipe Campos, Aníbal Matos, and Andry Maykol Pinto. Multi-domain mapping for offshore asset inspection using an autonomous surface vehicle. In *2020 IEEE International Conference on Autonomous Robot Systems and Competitions (ICARSC)*, pages 221–226, 2020. doi:10.1109/ICARSC49921.2020.9096097.

[28] Renato Jorge Silva, Pedro Nuno Leite, and Andry Maykol Pinto. Multi-agent optimization for offshore wind farm inspection using an improved population-based metaheuristic. In *2020 IEEE International Conference on Autonomous Robot Systems and Competitions (ICARSC)*, pages 53–60, 2020. doi:10.1109/ICARSC49921.2020.9096107.

[29] Diogo Ferreira Duarte, Maria Ines Pereira, and Andry Maykol Pinto. Multiple vessel detection in harsh maritime environments. *Marine Technology Society Journal*, 56(5):58–67, 2022. doi:https://doi.org/10.4031/MTSJ.56.5.07.

[30] Joohyun Woo and Nakwan Kim. Collision avoidance for an unmanned surface vehicle using deep reinforcement learning. *Ocean Engineering*, 199:107001, 3 2020. doi:10.1016/j.oceaneng.2020.107001.

[31] Yancai Hu, Xiangfei Meng, Qiang Zhang, and Gyei-Kark Park. A real-time collision avoidance system for autonomous surface vessel using fuzzy logic. *IEEE Access*, 8:108835–108846, 2020. doi:10.1109/ACCESS.2020.3001626.

[32] Renato Silva, Aníbal Matos, and Andry Maykol Pinto. Multi-criteria metric to evaluate motion planners for underwater intervention. *Autonomous Robots*, 46(8):971–983, 2022. doi:https://doi.org/10.1007/s10514-022-10060-x.

[33] Andry Maykol Pinto and Anibal C. Matos. Maresye: A hybrid imaging system for underwater robotic applications. *Information Fusion*, 55:16–29, 2020. doi:https://doi.org/10.1016/j.inffus.2019.07.014.

[34] H Ferreira, C Almeida, A Martins, J Almeida, N Dias, A Dias, and E Silva. Autonomous bathymetry for risk assessment with roaz robotic surface vehicle. pages 1–6, 2009. doi:10.1109/OCEANSE.2009.5278235.

[35] Alfredo Martins, Hugo Ferreira, Carlos Almeida, Hugo Silva, José Miguel Almeida, and Eduardo P. da Silva. Roaz and roaz ii autonomous surface vehicle design and implementation. 2007. URL: http://hdl.handle.net/10400.22/6974.

[36] N A Cruz and A C Matos. The mares auv, a modular autonomous robot for environment sampling. pages 1–6, 2008. doi:10.1109/OCEANS.2008.5152096.

[37] Daniel Filipe Campos, Anibal Matos, and Andry Maykol Pinto. Modular multi-domain aware autonomous surface vehicle for inspection. *IEEE Access*, 10:113355–113375, 2022. doi:10.1109/ACCESS.2022.3217504.

[38] Daniel Filipe Campos, Aníbal Matos, and Andry Maykol Pinto. Multi-domain inspection of offshore wind farms using an autonomous surface vehicle. *SN Applied Sciences*, 3:455, 4 2021. doi:10.1007/s42452-021-04451-5.

[39] A Utsav, A Abhishek, P Suraj, and R K Badhai. An iot based uav network for military applications. pages 122–125, 2021. doi:10.1109/WiSPNET51692.2021.9419470.

[40] Parthasarathy Velusamy, Santhosh Rajendran, Rakesh Kumar Mahendran, Salman Naseer, Muhammad Shafiq, and Jin-Ghoo Choi. Unmanned aerial vehicles (uav) in precision agriculture: Applications and challenges. *Energies*, 15(1), 2022. doi:https://doi.org/10.3390/en15010217.

[41] Maher Aljehani and Masahiro Inoue. Multi-uav tracking and scanning systems in m2m communication for disaster response. In *2016 IEEE 5th Global Conference on Consumer Electronics*, pages 1–2, 2016. doi:10.1109/GCCE.2016.7800524.

[42] Hanno Hildmann and Ernö Kovacs. Review: Using unmanned aerial vehicles (uavs) as mobile sensing platforms (msps) for disaster response, civil security and public safety. *Drones*, 3(3), 2019. doi:https://doi.org/10.3390/drones3030059.

[43] M Mozaffari, W Saad, M Bennis, Y H. Nam, and M Debbah. A tutorial on uavs for wireless networks: Applications, challenges, and open problems. *IEEE Communications Surveys Tutorials*, 21:2334–2360, 2019. doi:10.1109/COMST.2019.2902862.

[44] Francisco Soares Neves, Rafael Marques Claro, and Andry Maykol Pinto. End-to-end detection of a landing platform for offshore uavs based on a multimodal early fusion approach. *Sensors*, 23(5), 2023. doi:10.3390/s23052434.

[45] Kiam Heong Ang, G. Chong, and Yun Li. Pid control system analysis, design, and technology. *IEEE Transactions on Control Systems Technology*, 13:559–576, 7 2005. doi:10.1109/TCST.2005.847331.